

Joint Beamforming and Antenna Position Optimization for Fluid Antenna-Assisted MU-MIMO Networks

Tianyi Liao, *Graduate Student Member, IEEE*, Wei Guo, *Member, IEEE*, Hengtao He, *Member, IEEE*, Shenghui Song, *Senior Member, IEEE*, Jun Zhang, *Fellow, IEEE*, Khaled B. Letaief, *Fellow, IEEE*

Abstract—The fluid antenna system (FAS) has emerged as a disruptive technology for future wireless networks, offering unprecedented degrees of freedom (DoF) through the dynamic configuration of antennas in response to propagation environment variations. The integration of fluid antennas (FAs) with multiuser multiple-input multiple-output (MU-MIMO) networks promises substantial weighted sum rate (WSR) gains via joint beamforming and FA position optimization. However, the joint design is challenging due to the strong coupling between beamforming matrices and antenna positions. To address the challenge, we propose a novel block coordinate ascent (BCA)-based method in FA-assisted MU-MIMO networks. Specifically, we first employ matrix fractional programming techniques to reformulate the original complex problem into a more tractable form. Then, we solve the reformulated problem following the BCA principle, where we develop a low-complexity majorization maximization algorithm capable of optimizing all FA positions simultaneously. To further reduce the computational, storage, and interconnection costs, we propose a decentralized implementation for our proposed algorithm by utilizing the decentralized baseband processing (DBP) architecture. Simulation results demonstrate that with our proposed algorithm, the FA-assisted MU-MIMO system achieves up to a 47% WSR improvement over conventional MIMO networks equipped with fixed-position antennas. Moreover, the decentralized implementation reduces computation time by approximately 70% and has similar performance compared with the centralized implementation.

Index Terms—Fluid antenna system (FAS), MU-MIMO, fractional programming (FP), majorization maximization (MM), decentralized baseband processing (DBP).

I. INTRODUCTION

The sixth-generation (6G) wireless communication systems are expected to revolutionize global connectivity by enabling applications such as digital twins, precision healthcare, edge intelligence, and extended reality (XR) [1], [2]. These applications impose unprecedented requirements including terabit-per-second data rates, high energy efficiency, and sub-millisecond latency [3], [4]. To achieve these objectives, massive multiple-input multiple-output (MIMO) and multiuser MIMO (MU-MIMO) technology [5], [6] will play pivotal roles. The major advantage of MIMO systems is their ability to leverage spatial degrees of freedom (DoF), which can improve the system performance to exploit spatial diversity and multiplexing gains [7]. However, conventional MIMO systems typically assume fixed-position antenna (FPA) configurations, which lack the flexibility to dynamically adapt to changing propagation environments and thus cannot fully exploit the

spatial DoF. Specifically, some antennas inevitably experience deep fading and may suffer from high interference, leading to significant performance loss.

To address these challenges, the fluid antenna system (FAS) was proposed in [8] as a disruptive technology. FAS utilizes fluid antennas (FAs) to achieve flexible control over the positions, gains, radiation patterns, and other characteristics of the antennas [9]. Among these techniques, position optimization has been an efficient way to fully harness the spatial DoF. The advantages of utilizing FAs in MU-MIMO networks are twofold. On one hand, the position of the FAs can be changed to avoid deep fading channels for the desirable links, thereby improving the optimal diversity-multiplexing tradeoff [10]. On the other hand, FAs can mitigate multiuser interference (MUI) by optimizing antenna positions because interference experiences deep fade with proper adjustments [11]–[13].

A. Related Work

The concept of FAS was first introduced to wireless communications in [8]. Shortly after, a more precise definition of FAS and a channel model for single-antenna discrete port selection were proposed in [9]. The FAS with discrete port selection can be implemented by switchable pixels [14], and demonstrated superior performance over FPA systems [10], [15]–[19]. Although the discrete design simplifies hardware implementation, its performance is limited by the granularity of predefined ports. To address the challenge, an FAS with continuous position optimization implemented by liquid materials was proposed [20], [21]. However, such FAS still fails to fully harness spatial DoF, as it only allows a single FA to move along a one-dimensional line. Thus, the implementation of motor-driven FAS was later introduced in [22], [23], enabling continuous position optimization and seamless integration into MIMO systems. The advantages of motor-driven FAS were demonstrated in [24], where the authors analyzed an FA-assisted point-to-point MIMO system. By deriving the outage probability in closed form and numerically computing the system capacity gain, the authors proved that the motor-driven FAS offers higher stability and an increased data rate. Therefore, we focus on the motor-driven FAS in this paper.

Optimizing FA positions is key to unlocking the full potential of FAS. The first FA position optimization algorithm was introduced in [23]. The authors addressed the FA position optimization in a point-to-point MIMO system by formulating a non-concave optimization problem and solving it with a successive concave approximation (SCA)-based algorithm. However, this work did not consider joint beamforming and FA position optimization. Due to the strong coupling between beamforming matrices and FA positions, the SCA-based ap-

The authors are with the Department of Electronic and Computer Engineering, Hong Kong University of Science and Technology, Hong Kong. Emails: ty.liao@connect.ust.hk, {eeweigu, eehthe, eeshsong, eejzhang, eekhaled}@ust.hk.

proach cannot be directly applied to this joint optimization problem. To address this challenge, the authors of [25] studied a secure rate maximization problem with joint beamforming, FA position control, and artificial noise optimization problem. Then, they proposed the minimum mean square error (MMSE) method to decouple the optimization variables, demonstrating that the joint optimization significantly improves performance. The FAS was further extended to multiuser systems by [12], where the authors considered the transmit power minimization problem in an FA-assisted multiuser system with joint beamforming and FA position optimization. They decoupled the variables using zero-forcing (ZF) and MMSE methods. Then, they optimized FA positions via a multi-directional descent (MDD) framework. It was demonstrated that FAS can effectively cancel MUI, thereby significantly reducing transmit power while ensuring the data rate. More recently, [26] evaluated the system capacity gain of the FAS by solving the weighted sum rate (WSR) maximization problem in an FA-assisted downlink MU-multiple-input single-output (MISO) system. The authors first applied the weighted minimum mean square error (WMMSE) algorithm to decouple beamforming vectors and FA positions. Then, they leveraged the majorization maximization (MM) framework to solve the resulting non-concave FA position optimization problem. Simulation results demonstrated that FAS enhances overall system capacity in MU-MISO networks.

However, the MM framework in [26] has unaffordable complexity when the number of FAs at the BS is large. Specifically, the MM framework optimizes one FA position at a time while keeping the others fixed in each iteration, leading to the increased computational time as the number of FAs grows.

B. Contributions

In this paper, we propose a novel block coordinate ascent (BCA)-based algorithm for joint beamforming and FA position optimization in the FA-assisted downlink MU-MIMO system, as well as provide a decentralized implementation of the proposed algorithm. Our contributions are summarized as follows.

- Different from [26] that focuses on MU-MISO networks, we consider the more general FA-assisted MU-MIMO networks. We formulate the joint beamforming and antenna position optimization as a WSR maximization problem, where the objective function is non-concave and the optimization variables are highly coupled. To decouple the beamforming matrices and FA positions, we utilize two matrix fractional programming (FP) techniques, i.e., the quadratic transform and the Lagrangian dual transform [27], [28]. These FP techniques enable us to solve the decoupled subproblems by a BCA-based algorithm.
- Unlike existing FA position optimization algorithms that sequentially update FA positions, we propose a novel optimization algorithm based on the MM framework that optimizes all FA positions simultaneously. The proposed algorithm reduces computational time by exploiting parallelism and can be easily extended to a decentralized implementation. Additionally, we introduce a box-constrained movement mode to simplify both the formulated problem and the engineering implementation of FAS. This movement mode provides closed-form so-

lutions to reduce complexity and enables decentralized implementation by allowing the independent movement of each FA.

- To further reduce computational, storage, and interconnection costs, we propose a decentralized implementation of our algorithm by utilizing the decentralized baseband processing (DBP) architecture [29], which partitions the transmit FA array into several clusters. The DBP architecture can decompose the optimization problem into smaller subproblems, and enable decentralized units (DUs) to solve them in parallel. To enable the decentralized implementation of the proposed BCA-based algorithm, we employ the non-homogeneous transform and Nesterov's extrapolation [30], [31] to avoid the matrix inversion in the optimization of beamforming matrices. The decentralized implementation can significantly alleviate computational, storage, and interconnection costs with negligible performance loss.
- We conduct various numerical experiments to verify the performance of our proposed algorithm. It is shown that the proposed algorithm can improve the WSR of FA-assisted MU-MIMO networks by 47% compared with conventional MIMO networks using FPs. Moreover, the decentralized implementation reduces computation time by approximately 70% and has similar performance compared with the centralized implementation.

The remainder of this paper is organized as follows. Section II presents the channel model of the FA-assisted MU-MIMO system and formulates the WSR problem. Section III reformulates the problem using FP techniques and solves it using BCA and MM. The decentralized implementation of the proposed algorithm is introduced in Section IV. Simulation results are provided in Section V, and conclusions are drawn in Section VI.

Notation: Italic letters, boldface lowercase letters, and boldface uppercase letters denote scalars, vectors, and matrices, respectively. The imaginary unit is denoted by j . For a complex number a , its amplitude and phase are given by $|a|$ and $\angle a$, respectively. The ℓ_2 norm of a vector \mathbf{a} is $\|\mathbf{a}\|_2$. $[\mathbf{A}]_m$, $[\mathbf{A}]_{mn}$, \mathbf{A}^\top , \mathbf{A}^H , $\det(\mathbf{A})$, $\text{tr}(\mathbf{A})$, $\text{vec}(\mathbf{A})$, $\|\mathbf{A}\|_\infty$, and $\|\mathbf{A}\|_F$ denote the m -th row, the (m, n) -th element, transpose, conjugate transpose, determinant, trace, vectorization, the infinity norm, and the Frobenius norm of matrix \mathbf{A} , respectively. $\mathbf{A} \succeq \mathbf{0}$ and $\mathbf{A} \succ \mathbf{0}$ indicate that \mathbf{A} is positive semi-definite and positive definite, respectively. $\mathbb{C}^{M \times N}$, $\mathbb{R}^{M \times N}$, and $\mathbb{R}_+^{M \times N}$ denote the sets of $M \times N$ complex, real, and non-negative real matrices, respectively. The circularly symmetric complex Gaussian (CSCG) distribution with zero mean and covariance $\sigma^2 \mathbf{I}$ is represented as $\mathcal{CN}(\mathbf{0}, \sigma^2 \mathbf{I})$, and the uniform distribution over $[a, b]$ is denoted by $\mathcal{U}[a, b]$. Operator $\partial(\cdot)$ denotes the partial differential. $\nabla_{\mathbf{x}} f(\mathbf{x})$ and $\nabla_{\mathbf{x}}^2 f(\mathbf{x})$ denote the gradient vector and Hessian matrix of $f(\mathbf{x})$ with respect to (w.r.t.) \mathbf{x} respectively.

II. SYSTEM MODEL AND PROBLEM FORMULATION

As shown in Fig. 1, we consider a downlink MU-MIMO system where a BS with M FAs serves K users, each equipped with N FAs. A three-dimensional (3D) Cartesian coordinate system is established to describe the positions of the transmit FAs at the BS and receive FAs at the users.

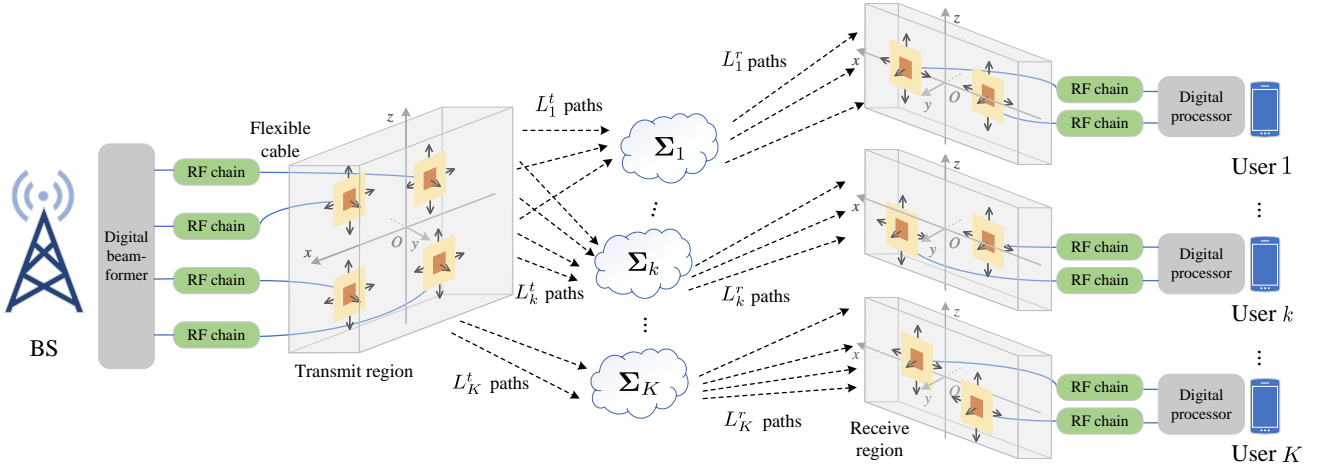


Fig. 1. The 3D FA-assisted MU-MIMO wireless communication network.

Specifically, let $\mathbf{t}_m = [x_m^t, y_m^t, z_m^t]^T \in \mathcal{C}_m^t$, $1 \leq m \leq M$, denote the position of m -th transmit FA at the BS and let $\mathbf{r}_{kn} = [x_{kn}^r, y_{kn}^r, z_{kn}^r]^T \in \mathcal{C}_{kn}^r$, $1 \leq k \leq K$, $1 \leq n \leq N$, denote the position of the n -th receive FA at user k , where \mathcal{C}_m^t and \mathcal{C}_{kn}^r are the given 3D movable regions of transmit and receive FAs. Without loss of generality, the movable regions are assumed to be cuboid [12], i.e., $\mathcal{C}_m^t = [x_m^{\min}, x_m^{\max}] \times [y_m^{\min}, y_m^{\max}] \times [z_m^{\min}, z_m^{\max}]$ and $\mathcal{C}_{kn}^r = [x_{kn}^{\min}, x_{kn}^{\max}] \times [y_{kn}^{\min}, y_{kn}^{\max}] \times [z_{kn}^{\min}, z_{kn}^{\max}]$, $\forall k, n$, where we assume the FA movable regions of the K users to be identical.

In this paper, we consider narrow-band slow fading channels, where the transmit and receive FAs remain static or move slowly within the movable region during each quasi-static fading block. Moreover, the time required for FA movement is assumed to be much shorter than the coherence time [23]. Let $\mathbf{s}_k \in \mathbb{C}^d$ denote the data stream desired by user k , where $d \leq \min\{M, N\}$ is the number of parallel data streams, and assume that $\mathbf{s}_k \sim \mathcal{CN}(\mathbf{0}, \mathbf{I})$. Define $\mathbf{W}_k \in \mathbb{C}^{M \times d}$ as the beamforming matrix for transmitting data \mathbf{s}_k from the BS to user k . The received signal \mathbf{y}_k at user k is given by

$$\mathbf{y}_k = \mathbf{H}_k(\mathbf{T}, \mathbf{R}_k) \mathbf{W}_k \mathbf{s}_k + \sum_{j=1, j \neq k}^K \mathbf{H}_k(\mathbf{T}, \mathbf{R}_k) \mathbf{W}_j \mathbf{s}_j + \mathbf{n}_k, \quad (1)$$

where $\mathbf{T} = [\mathbf{t}_1, \dots, \mathbf{t}_M]^T \in \mathbb{R}^{M \times 3}$ and $\mathbf{R}_k = [\mathbf{r}_{k1}, \dots, \mathbf{r}_{kN}]^T \in \mathbb{R}^{N \times 3}$ represent the positions of the transmit FAs at the BS and the receive FAs at user k , respectively. The channel matrix between the BS and user k is given as $\mathbf{H}_k(\mathbf{T}, \mathbf{R}_k) \in \mathbb{C}^{N \times M}$, which depends on both \mathbf{T} and \mathbf{R}_k . The term $\mathbf{n}_k \in \mathbb{C}^N$ denotes additive white Gaussian noise following the distribution $\mathcal{CN}(\mathbf{0}, \sigma_k^2 \mathbf{I})$.

A. Channel Model

In this paper, we assume that the movable regions at both the users and the BS are much smaller than the signal propagation distance, ensuring the far-field condition. Therefore, the angle of departure (AoD), the angle of arrival (AoA), and the amplitude of the complex gain for each channel path remain unchanged regardless of the FA positions. In contrast, the phase of each channel path depends on the FA positions and varies accordingly [24].

Let L_k^t and L_k^r , $1 \leq k \leq K$, denote the numbers of transmit and receive channel paths between the BS and user k , respectively. The elevation and azimuth AoDs of the i -th transmit path are denoted by θ_{ki}^t and ϕ_{ki}^t , where $1 \leq i \leq L_k^t$. Similarly, the elevation and azimuth AoAs of the j -th receive path are denoted by θ_{kj}^r and ϕ_{kj}^r , where $1 \leq j \leq L_k^r$. Therefore, the steering vectors corresponding to the directions of the i -th transmit and j -th receive paths are given by

$$\mathbf{g}_{ki}^t = [\cos \theta_{ki}^t \cos \phi_{ki}^t, \cos \theta_{ki}^t \sin \phi_{ki}^t, \sin \theta_{ki}^t]^T, \quad (2)$$

$$\mathbf{f}_{kj}^r = [\cos \theta_{kj}^r \cos \phi_{kj}^r, \cos \theta_{kj}^r \sin \phi_{kj}^r, \sin \theta_{kj}^r]^T, \quad (3)$$

with $1 \leq k \leq K$, $1 \leq i \leq L_k^t$, and $1 \leq j \leq L_k^r$, respectively. Then, for the i -th transmit channel path from the BS to user k , the distance difference between the path originating from the m -th BS antenna position \mathbf{t}_m and that from the origin of the BS coordinate system \mathbf{o} is given by

$$\rho_{ki}^t(\mathbf{t}_m) \triangleq \mathbf{g}_{ki}^t(\mathbf{t}_m - \mathbf{o}) \quad (4)$$

$$= x_m^t \cos \theta_{ki}^t \cos \phi_{ki}^t + y_m^t \cos \theta_{ki}^t \sin \phi_{ki}^t + z_m^t \sin \theta_{ki}^t.$$

Similarly, for the j -th receive channel path from the BS to user k , the distance difference between the path originating from the n -th receive antenna position \mathbf{r}_{kn} and that from the origin of user k 's coordinate system \mathbf{o}_k is given by

$$\rho_{kj}^r(\mathbf{r}_{kn}) \triangleq \mathbf{f}_{kj}^r(\mathbf{r}_{kn} - \mathbf{o}_k) \quad (5)$$

$$= x_{kn}^r \cos \theta_{kj}^r \cos \phi_{kj}^r + y_{kn}^r \cos \theta_{kj}^r \sin \phi_{kj}^r + z_{kn}^r \sin \theta_{kj}^r.$$

Let λ denote the carrier wavelength. For the i -th transmit (and j -th receive) channel paths from the BS to user k , the phase differences between the path originating from \mathbf{t}_m and that from \mathbf{o}_m (and between the path originating from \mathbf{r}_{kn} and that from \mathbf{o}_{kn}) are given by $2\pi \rho_{ki}^t(\mathbf{t}_m)/\lambda$ and $2\pi \rho_{kj}^r(\mathbf{r}_{kn})/\lambda$, respectively. Hence, the transmit and receive field-response vectors (FRVs) for the channel between the BS and user k are given by [12], [23]

$$\mathbf{g}_k(\mathbf{t}_m) \triangleq \left[e^{j \frac{2\pi}{\lambda} \rho_{k,1}^t(\mathbf{t}_m)}, e^{j \frac{2\pi}{\lambda} \rho_{k,2}^t(\mathbf{t}_m)}, \dots, e^{j \frac{2\pi}{\lambda} \rho_{k,L_k^t}^t(\mathbf{t}_m)} \right]^T, \quad (6)$$

$$\mathbf{f}_k(\mathbf{r}_{kn}) \triangleq \left[e^{j \frac{2\pi}{\lambda} \rho_{k,1}^r(\mathbf{r}_{kn})}, e^{j \frac{2\pi}{\lambda} \rho_{k,2}^r(\mathbf{r}_{kn})}, \dots, e^{j \frac{2\pi}{\lambda} \rho_{k,L_k^r}^r(\mathbf{r}_{kn})} \right]^T, \quad (7)$$

with $1 \leq k \leq K$, $1 \leq m \leq M$, and $1 \leq n \leq N$.

Besides, we define the path-response matrix (PRM) $\Sigma_k \in$

$\mathbb{C}^{L_k^r \times L_k^t}$ as the response between each pair of transmit and receive channel paths from the BS to user k . The entry $[\Sigma_k]_{ji}$ represents the response between the i -th transmit and j -th receive paths for user k . Thus, $\mathbf{H}_k(\mathbf{T}, \mathbf{R}_k)$ is given by

$$\mathbf{H}_k(\mathbf{T}, \mathbf{R}_k) = \mathbf{F}_k^H(\mathbf{R}_k) \Sigma_k \mathbf{G}_k(\mathbf{T}), \quad (8)$$

where $\mathbf{F}_k(\mathbf{R}_k) = [\mathbf{f}_k(\mathbf{r}_{k,1}), \dots, \mathbf{f}_k(\mathbf{r}_{kn})] \in \mathbb{C}^{L_k^r \times N}$ and $\mathbf{G}_k(\mathbf{T}) = [\mathbf{g}_k(\mathbf{t}_1), \dots, \mathbf{g}_k(\mathbf{t}_M)] \in \mathbb{C}^{L_k^t \times M}$ denote the field response matrices (FRMs) of all the receive FAs at user k and those at the BS, respectively.

B. Problem Formulation

A fundamental problem in MU-MIMO downlink transmission is WSR maximization. The WSR is defined as

$$R = \sum_{k=1}^K \alpha_k R_k, \quad (9)$$

where the weight α_k denotes the priority of user k , and R_k is the achievable rate of user k , given by [32], [33]

$$R_k = \log \det (\mathbf{I} + \mathbf{W}_k^H \mathbf{H}_k^H(\mathbf{T}, \mathbf{R}_k) \mathbf{M}_k^{-1} \mathbf{H}_k(\mathbf{T}, \mathbf{R}_k) \mathbf{W}_k). \quad (10)$$

The interference-plus-noise matrix \mathbf{M}_k is defined as

$$\mathbf{M}_k = \sum_{j=1, j \neq k}^K \mathbf{H}_k(\mathbf{T}, \mathbf{R}_k) \mathbf{W}_j \mathbf{W}_j^H \mathbf{H}_k^H(\mathbf{T}, \mathbf{R}_k) + \sigma_k^2 \mathbf{I}. \quad (11)$$

Let $\underline{\mathbf{W}} = \{\mathbf{W}_k, \forall k\}$ denote the set of beamforming matrices, and $\underline{\mathbf{R}} = \{\mathbf{R}_k, \forall k\}$ denote the set of all receive FA positions. Then, we can formulate the optimization problem as

$$\max_{\underline{\mathbf{W}}, \underline{\mathbf{T}}, \underline{\mathbf{R}}} R \quad (12a)$$

$$\text{s. t.} \quad \sum_{k=1}^K \text{tr}(\mathbf{W}_k \mathbf{W}_k^H) \leq P_{\max}, \quad (12b)$$

$$\mathbf{t}_m \in \mathcal{C}_m^t, \quad \forall m, \quad (12c)$$

$$\mathbf{r}_{kn} \in \mathcal{C}_{kn}^r, \quad \forall kn, \quad (12d)$$

$$\|\mathbf{t}_m - \mathbf{t}_{m'}\|_2 \geq D, \quad 1 \leq m, m' \leq M, m \neq m', \quad (12e)$$

$$\|\mathbf{r}_{kn} - \mathbf{r}_{kn'}\|_2 \geq D, \quad \forall k, 1 \leq n, n' \leq N, n \neq n'. \quad (12f)$$

Here, the constraint (12b) denotes the total transmit power constraint, where P_{\max} is the total transmit power budget at the BS. Constraints (12c) and (12d) guarantee the FAs at the BS and users remain within the movable regions. Constraints (12e) and (12f) prevent coupling effects between any pair of FAs at the BS and users, respectively. The problem (12) is difficult to solve because the objective function (12a) is highly nonlinear and non-concave with respect to (w.r.t.) the beamforming matrices $\underline{\mathbf{W}}$ and the FA positions $\underline{\mathbf{T}}$ and $\underline{\mathbf{R}}$. Additionally, the

optimization variables are highly coupled, making the problem more intractable.

III. BLOCK COORDINATE ASCENT (BCA)-BASED ALGORITHM

In this section, we propose a BCA-based algorithm to the problem (12). First, we employ the FP method to decouple the variables in the problem (12). Then, the MM algorithm is utilized to address the non-concave optimization of FA positions.

A. Problem Reformulation

To solve the complicated problem (12), we first reformulate it using the widely adopted FP method [27]. Specifically, since the objective function (12a) is a sum-of-functions-of-matrix-ratios, we apply the matrix FP framework developed in [34], detailed as follows.

First, applying the matrix Lagrangian dual transform [34, Theorem 2] to the problem (12) allows us to extract the ratios from the logarithms in (10). Therefore, the problem (12) can be reformulated as

$$\max_{\underline{\mathbf{W}}, \underline{\mathbf{T}}, \underline{\mathbf{R}}, \underline{\Gamma}} f_{\text{Lag}}(\underline{\mathbf{W}}, \underline{\mathbf{T}}, \underline{\mathbf{R}}, \underline{\Gamma}) \quad (13a)$$

$$\text{s. t.} \quad (12b) - (12f), \quad (13b)$$

where $f_{\text{Lag}}(\underline{\mathbf{W}}, \underline{\mathbf{T}}, \underline{\mathbf{R}}, \underline{\Gamma})$ is given by (14) at the bottom of the page, and $\underline{\Gamma} = \{\Gamma_k, \forall k\}$ denotes the set of auxiliary variables.

By applying the matrix quadratic transform [34, Theorem 1] to the problem (13), we can further decouple the ratios in the reformulated objective function (14) and reformulate the problem (13) as

$$\max_{\underline{\mathbf{W}}, \underline{\mathbf{T}}, \underline{\mathbf{R}}, \underline{\Gamma}, \underline{\Phi}} f_{\text{Quad}}(\underline{\mathbf{W}}, \underline{\mathbf{T}}, \underline{\mathbf{R}}, \underline{\Gamma}, \underline{\Phi}) \quad (15a)$$

$$\text{s. t.} \quad (12b) - (12f), \quad (15b)$$

where $f_{\text{Quad}}(\underline{\mathbf{W}}, \underline{\mathbf{T}}, \underline{\mathbf{R}}, \underline{\Gamma}, \underline{\Phi})$ is given by (16) at the bottom of the page, and $\underline{\Phi} = \{\Phi_k, \forall k\}$ denotes the set of auxiliary variables.

With the above FP-based two-step transformation, the original problem (12) is equivalent to the problem (15). Then we employ the BCA algorithm to solve the problem (15) by iteratively optimizing one set of variables while keeping others fixed until convergence.

B. The Update Step of $\underline{\Gamma}$ and $\underline{\Phi}$

In this step, we aim to optimize the auxiliary variables $\underline{\Gamma}$ and $\underline{\Phi}$ with the fixed $\underline{\mathbf{W}}$, $\underline{\mathbf{T}}$, and $\underline{\mathbf{R}}$. The optimal solution of $\underline{\Gamma}$ and $\underline{\Phi}$ are derived by setting the first-order derivatives of (16) to zero w.r.t. Γ_k and Φ_k , respectively. Let $\bar{\mathbf{W}}_k$, $\bar{\mathbf{T}}$, $\bar{\mathbf{R}}_k$, $\bar{\Gamma}_k$, and let $\bar{\Phi}_k$ denote the temporal optimization results obtained by the previous iteration, and let $\bar{\mathbf{M}}_k$ denote the temporal

$$f_{\text{Lag}}(\underline{\mathbf{W}}, \underline{\mathbf{T}}, \underline{\mathbf{R}}, \underline{\Gamma}) = \sum_{k=1}^K \alpha_k \left(\log \det (\mathbf{I} + \Gamma_k) - \text{tr}(\Gamma_k) + \text{tr} \left((\mathbf{I} + \Gamma_k) \mathbf{W}_k^H \mathbf{H}_k^H(\mathbf{T}, \mathbf{R}_k) \right. \right. \\ \left. \left. \times \left(\sum_{j=1}^K \mathbf{H}_k(\mathbf{T}, \mathbf{R}_j) \mathbf{W}_j \mathbf{W}_j^H \mathbf{H}_k^H(\mathbf{T}, \mathbf{R}_j) + \sigma_k^2 \mathbf{I} \right)^{-1} \mathbf{H}_k(\mathbf{T}, \mathbf{R}_k) \mathbf{W}_k \right) \right). \quad (14)$$

$$f_{\text{Quad}}(\underline{\mathbf{W}}, \underline{\mathbf{T}}, \underline{\mathbf{R}}, \underline{\Gamma}, \underline{\Phi}) = \sum_{k=1}^K \left(\alpha_k \log \det (\mathbf{I} + \Gamma_k) - \alpha_k \text{tr}(\Gamma_k) + \text{tr} \left((\mathbf{I} + \Gamma_k) \left(\sqrt{\alpha_k} \mathbf{W}_k^H \mathbf{H}_k^H(\mathbf{T}, \mathbf{R}_k) \Phi_k \right. \right. \right. \\ \left. \left. \left. + \sqrt{\alpha_k} \Phi_k^H \mathbf{H}_k(\mathbf{T}, \mathbf{R}_k) \mathbf{W}_k - \Phi_k^H \left(\sum_{j=1}^K \mathbf{H}_k(\mathbf{T}, \mathbf{R}_j) \mathbf{W}_j \mathbf{W}_j^H \mathbf{H}_k^H(\mathbf{T}, \mathbf{R}_j) + \sigma_k^2 \mathbf{I} \right) \Phi_k \right) \right) \right). \quad (16)$$

interference-plus-noise matrix. The closed-form expressions for the optimal Φ_k and Γ_k are given by [34]

$$\Phi_k = \sqrt{\alpha_k} \left(\bar{\mathbf{M}}_k + \bar{\mathbf{H}}_k \bar{\mathbf{W}}_k \bar{\mathbf{W}}_k^H \bar{\mathbf{H}}_k^H \right)^{-1} \bar{\mathbf{H}}_k \bar{\mathbf{W}}_k, \quad (17)$$

$$\Gamma_k = \bar{\mathbf{W}}_k^H \bar{\mathbf{H}}_k^H \bar{\mathbf{M}}_k^{-1} \bar{\mathbf{H}}_k \bar{\mathbf{W}}_k, \quad (18)$$

respectively, where we define $\bar{\mathbf{H}}_k \triangleq \mathbf{H}_k(\bar{\mathbf{T}}, \bar{\mathbf{R}}_k)$.

C. The Update Step of \mathbf{W}

In this step, we aim to optimize the beamforming matrices \mathbf{W} with the fixed \mathbf{T} , \mathbf{R} , $\mathbf{\Gamma}$, and $\mathbf{\Phi}$. Then, the optimization problem (15) reduces to

$$\max_{\mathbf{W}} f_{\text{Quad}}(\mathbf{W}) \quad \text{s. t. (12b),} \quad (19)$$

where $f_{\text{Quad}}(\mathbf{W}) = f_{\text{Quad}}(\mathbf{W}, \bar{\mathbf{T}}, \bar{\mathbf{R}}, \bar{\mathbf{\Gamma}}, \bar{\mathbf{\Phi}})$. As derived in [34], the optimal solution to the problem (19) is given by

$$\mathbf{W}_k = \left(\sum_{j=1}^K \bar{\mathbf{H}}_j^H \bar{\mathbf{\Phi}}_j (\mathbf{I} + \bar{\mathbf{\Gamma}}_j) \bar{\mathbf{\Phi}}_j^H \bar{\mathbf{H}}_j + \mu \mathbf{I} \right)^{-1} \times \sqrt{\alpha_k} \bar{\mathbf{H}}_k^H \bar{\mathbf{\Phi}}_k (\mathbf{I} + \bar{\mathbf{\Gamma}}_k), \quad (20)$$

where $\mu \geq 0$ is computed via bisection search to ensure that $\bar{\mathbf{W}}$ can satisfy the complementary slackness condition of the power budget constraint (12b) [35].

D. The Update Step of \mathbf{T}

In this step, we aim to optimize the positions of the transmit FAs at the BS \mathbf{T} with the fixed \mathbf{W} , \mathbf{R} , $\mathbf{\Gamma}$, and $\mathbf{\Phi}$. Then, the optimization problem (15a) reduces to

$$\max_{\mathbf{T}} f_{\text{Quad}}(\mathbf{T}) \quad \text{s. t. (12c), (12e).} \quad (21)$$

Unlike the update steps for $\mathbf{\Gamma}$, $\mathbf{\Phi}$, and \mathbf{W} , the objective function $f_{\text{Quad}}(\mathbf{T})$ remains nonconcave w.r.t. \mathbf{T} . The MM algorithm [36] effectively solves this non-concave problem by iteratively finding a series of concave lower bounds for the non-concave function $f_{\text{Quad}}(\mathbf{T})$, known as the *surrogate function*. A key advantage of the MM algorithm is its convergence guarantee, which is discussed in the sequel.

To solve the problem (21) using the MM algorithm, the optimal value of \mathbf{T} is computed iteratively. Each MM iteration consists of a *majorization step*, followed by a *maximization step*. In the *majorization step*, the *surrogate function* is computed as

$$h^{\text{Tx}}(\mathbf{T}|\bar{\mathbf{T}}) \leq f_{\text{Quad}}(\mathbf{T}), \quad (22)$$

where Tx indicates the update step is related to \mathbf{T} , and $\bar{\mathbf{T}}$ denotes a constant satisfying (12c) and (12e). In the *maximization step*, we determine the optimal \mathbf{T} subject to the given constraints as

$$\max_{\mathbf{T}} h^{\text{Tx}}(\mathbf{T}|\bar{\mathbf{T}}), \quad \text{s. t. (12c), (12e).} \quad (23)$$

In each MM iteration, after constructing a distinct *surrogate function*, we obtain a new optimum accordingly. Then, the update step of \mathbf{T} for the proposed MM algorithm is executed until convergence. The convergence of MM method is ensured because $f_{\text{Quad}}(\mathbf{T})$ remains non-decreasing after each MM iteration, as

$$f_{\text{Quad}}(\mathbf{T}) \geq h^{\text{Tx}}(\mathbf{T}|\bar{\mathbf{T}}) \geq h^{\text{Tx}}(\bar{\mathbf{T}}|\bar{\mathbf{T}}) = f_{\text{Quad}}(\bar{\mathbf{T}}), \quad (24)$$

where $\bar{\mathbf{T}}$ is the solution to the problem (23). The first inequality follows from (22), the second inequality holds since $\bar{\mathbf{T}}$ is the optimal solution to the problem (23), and the last equality results from the equality condition of (22).

The key to applying the MM algorithm is constructing a suitable surrogate function. Here, we introduce the following lemma to construct the surrogate function that locally approximates the objective function [36].

Lemma 1. *Let $f : \mathbb{R}^n \rightarrow \mathbb{R}$ be a continuously differentiable function with bounded curvature, i.e., there exists a matrix \mathbf{L} such that $\mathbf{L} \succeq \nabla^2 f(\mathbf{x})$, $\forall \mathbf{x} \in \mathcal{X}$. Then,*

$$f(\mathbf{x}) \geq f(\bar{\mathbf{x}}) + \nabla f^T(\bar{\mathbf{x}}) (\mathbf{x} - \bar{\mathbf{x}}) - \frac{1}{2} (\mathbf{x} - \bar{\mathbf{x}})^T \mathbf{L} (\mathbf{x} - \bar{\mathbf{x}}), \quad (25)$$

where $\bar{\mathbf{x}}$ is a constant satisfying $\bar{\mathbf{x}} \in \mathcal{X}$.

By directly applying Lemma 1 to $f_{\text{Quad}}(\mathbf{T})$ and letting $\mathbf{L} = \delta^{\text{Tx}} \mathbf{I}$ with

$$\delta^{\text{Tx}} \geq \lambda_{\max} \left(\nabla_{\text{vec}(\mathbf{T})}^2 f_{\text{Quad}}(\mathbf{T}) \right), \quad (26)$$

for any given \mathbf{T} satisfying (12c) and (12e), we can construct the surrogate function $h^{\text{Tx}}(\mathbf{T}|\bar{\mathbf{T}})$ as

$$\begin{aligned} h^{\text{Tx}}(\mathbf{T}|\bar{\mathbf{T}}) &= -\frac{\delta^{\text{Tx}}}{2} \text{vec}(\mathbf{T})^T \text{vec}(\mathbf{T}) \\ &+ \left(\nabla_{\text{vec}(\mathbf{T})} f_{\text{Quad}}^T(\bar{\mathbf{T}}) + \delta^{\text{Tx}} \text{vec}(\bar{\mathbf{T}})^T \right) \text{vec}(\mathbf{T}) + \text{const}, \end{aligned} \quad (27)$$

where the entries of $\nabla_{\text{vec}(\mathbf{T})} f_{\text{Quad}}(\mathbf{T})$ are given by

$$\frac{\partial f_{\text{Quad}}}{\partial x_m^t} = -\frac{4\pi}{\lambda} \sum_{k=1}^K \sum_{q=1}^{L_k^t} \left| [\mathbf{D}_k^{\text{Tx}}]_{mq} \right| \cos \theta_{kq}^t \cos \phi_{kq}^t \sin(\xi_{kmq}^{\text{Tx}}), \quad (28a)$$

$$\frac{\partial f_{\text{Quad}}}{\partial y_m^t} = -\frac{4\pi}{\lambda} \sum_{k=1}^K \sum_{q=1}^{L_k^t} \left| [\mathbf{D}_k^{\text{Tx}}]_{mq} \right| \cos \theta_{kq}^t \sin \phi_{kq}^t \sin(\xi_{kmq}^{\text{Tx}}), \quad (28b)$$

$$\frac{\partial f_{\text{Quad}}}{\partial z_m^t} = -\frac{4\pi}{\lambda} \sum_{k=1}^K \sum_{q=1}^{L_k^t} \left| [\mathbf{D}_k^{\text{Tx}}]_{mq} \right| \sin \theta_{kq}^t \sin(\xi_{kmq}^{\text{Tx}}), \quad (28c)$$

respectively. Here, \mathbf{D}_k^{Tx} and ξ_{kmq}^{Tx} are given by

$$\begin{aligned} \mathbf{D}_k^{\text{Tx}} &\triangleq \left(\frac{\partial f_{\text{Quad}}}{\partial \mathbf{G}_k} \right)^T = \sqrt{\alpha_k} \bar{\mathbf{W}}_k (\mathbf{I} + \bar{\mathbf{\Gamma}}_k) \bar{\mathbf{\Phi}}_k^H \bar{\mathbf{F}}_k^H \Sigma_k \\ &- \hat{\mathbf{W}} \mathbf{G}_k^H(\bar{\mathbf{T}}) \Sigma_k^H \bar{\mathbf{F}}_k \bar{\mathbf{\Phi}}_k (\mathbf{I} + \bar{\mathbf{\Gamma}}_k) \bar{\mathbf{\Phi}}_k^H \bar{\mathbf{F}}_k^H \Sigma_k \end{aligned} \quad (29)$$

and

$$\begin{aligned} \xi_{kmq}^{\text{Tx}} &= \angle [\mathbf{D}_k^{\text{Tx}}]_{mq} + \frac{2\pi}{\lambda} \left(x_m^t \cos \theta_{kq}^t \cos \phi_{kq}^t \right. \\ &\left. + y_m^t \cos \theta_{kq}^t \sin \phi_{kq}^t + z_m^t \sin \theta_{kq}^t \right), \end{aligned} \quad (30)$$

respectively, where we define $\bar{\mathbf{F}}_k \triangleq \mathbf{F}_k(\bar{\mathbf{R}}_k)$ and $\hat{\mathbf{W}} \triangleq \sum_{k=1}^K \bar{\mathbf{W}}_k \bar{\mathbf{W}}_k^H$. Moreover, by deriving an upper bound for the right hand side (r.h.s.) of (26) for any \mathbf{T} satisfying (12c) and (12e), we obtain the closed-form expression of δ^{Tx} as given by (31) at the bottom of the page. The detailed derivations of (28) and (31) are shown in Appendix A.

Although we have found the concave surrogate function (27), the constraint (12e) still makes the optimization

$$\delta^{\text{Tx}} = \max_{1 \leq m \leq M} \frac{24\pi^2}{\lambda^2} \sum_{k=1}^K L_k^t \left(\left(\sum_{j=1}^M |\hat{\mathbf{W}}_{mj}| + \sqrt{M} \|\hat{\mathbf{W}}_m\|_2 \right) \|\Sigma_k^H \bar{\mathbf{F}}_k \bar{\mathbf{\Phi}}_k (\mathbf{I} + \bar{\mathbf{\Gamma}}_k) \bar{\mathbf{\Phi}}_k^H \bar{\mathbf{F}}_k^H \Sigma_k\|_2 + \sqrt{\frac{\alpha_k}{L_k^t}} \|\bar{\mathbf{W}}_k\|_m (\mathbf{I} + \bar{\mathbf{\Gamma}}_k) \bar{\mathbf{\Phi}}_k^H \bar{\mathbf{F}}_k^H \Sigma_k\|_2 \right). \quad (31)$$

tion problem (23) nonconcave. Therefore, we apply Cauchy-Schwarz inequality to the left hand side (l.h.s.) of the constraint (12e) and obtain a linear constraint

$$\frac{(\bar{\mathbf{t}}_m - \bar{\mathbf{t}}_{m'})^\top (\mathbf{t}_m - \mathbf{t}_{m'})}{\|\bar{\mathbf{t}}_m - \bar{\mathbf{t}}_{m'}\|_2} \geq D, \quad \forall m \neq m'. \quad (32)$$

Thus, the original problem (21) can be formulated as

$$\max_{\mathbf{T}} h^{\text{Tx}}(\mathbf{T}|\bar{\mathbf{T}}), \quad \text{s. t. (12c), (32),} \quad (33)$$

which is a concave quadratic programming problem. As demonstrated in [23], solving (33) becomes simpler by initially assuming all constraints are inactive. This transformation simplifies the problem to an unconstrained quadratic optimization, whose closed-form solution is given by

$$\mathbf{T}^* = \bar{\mathbf{T}} + \frac{1}{\delta_{\text{Tx}}} \nabla_{\mathbf{T}} f_{\text{Quad}}(\bar{\mathbf{T}}). \quad (34)$$

Next, we verify this assumption by checking whether \mathbf{T}^* satisfies the constraints (12c) and (32). If the constraints are not satisfied, we apply the interior-point method [35] to obtain a valid optimum \mathbf{T}^* .

E. The Update Step of \mathbf{R}

In this step, our target is to optimize the positions of the receive FAs \mathbf{R} with fixed \mathbf{T} , \mathbf{W} , \mathbf{I} , and $\mathbf{\Phi}$. The objective function $f_{\text{Quad}}(\mathbf{R})$ is reformulated as

$$f_{\text{Quad}}(\mathbf{R}) = \sum_{k=1}^K f_{\text{Quad}}(\mathbf{R}_k). \quad (35)$$

Since the terms of the r.h.s. of (35) do not couple with each other, it is feasible to optimize $f_{\text{Quad}}(\mathbf{R}_k)$ independently. Therefore, we simply provide the update step of \mathbf{R}_k in the remainder of this subsection. Then, the optimization problem is reformulated as

$$\max_{\mathbf{R}_k} f_{\text{Quad}}(\mathbf{R}_k) \quad \text{s. t. (12d), (12f).} \quad (36)$$

Similar to the optimization step of \mathbf{T} , the objective function $f_{\text{Quad}}(\mathbf{R}_k)$ is non-concave w.r.t. \mathbf{R}_k . Hence, we utilize MM to optimize \mathbf{R}_k , and the problem (36) is reformulated as

$$\max_{\mathbf{R}_k} h_k^{\text{Rx}}(\mathbf{R}_k|\bar{\mathbf{R}}_k) \quad (37a)$$

s. t. (12d),

$$\frac{(\bar{\mathbf{r}}_{kn} - \bar{\mathbf{r}}_{kn'})^\top (\mathbf{r}_{kn} - \mathbf{r}_{kn'})}{\|\bar{\mathbf{r}}_{kn} - \bar{\mathbf{r}}_{kn'}\|_2} \geq D, \quad \forall n \neq n', \quad (37b)$$

where Rx indicates the update step relates to \mathbf{R} . The function $h_k^{\text{Rx}}(\mathbf{R}_k|\bar{\mathbf{R}}_k)$ is the *surrogate function* of $f_{\text{Quad}}(\mathbf{R}_k)$, given by

$$\begin{aligned} h_k^{\text{Rx}}(\mathbf{R}_k|\bar{\mathbf{R}}_k) &= -\frac{\delta_k^{\text{Rx}}}{2} \text{vec}(\mathbf{R}_k)^\top \text{vec}(\mathbf{R}_k) \\ &+ \left(\nabla_{\text{vec}(\mathbf{R}_k)} f_{\text{Quad}}^\top(\bar{\mathbf{R}}_k) + \delta_k^{\text{Rx}} \text{vec}(\bar{\mathbf{R}}_k)^\top \right) \text{vec}(\mathbf{R}_k) \\ &+ \text{const}, \quad (38) \end{aligned}$$

where δ_k^{Rx} needs to satisfy

$$\delta_k^{\text{Rx}} \geq \lambda_{\max} \left(\nabla_{\text{vec}(\mathbf{R}_k)}^2 f_{\text{Quad}}(\mathbf{R}_k) \right), \quad (39)$$

for any \mathbf{R}_k satisfying (12d) and (37b) according to Lemma 1.

The entries of the gradient $\nabla_{\text{vec}(\mathbf{R}_k)} f_{\text{Quad}}(\mathbf{R}_k)$ are given by

$$\frac{\partial f_{\text{Quad}}}{\partial x_{kn}^r} = -\frac{4\pi}{\lambda} \sum_{k=1}^K \sum_{q=1}^{L_k^r} \left| [\mathbf{D}_k^{\text{Rx}}]_{nq} \right| \cos \theta_{kq}^r \cos \phi_{kq}^r \sin(\xi_{knq}^{\text{Rx}}), \quad (40a)$$

$$\frac{\partial f_{\text{Quad}}}{\partial y_{kn}^r} = -\frac{4\pi}{\lambda} \sum_{k=1}^K \sum_{q=1}^{L_k^r} \left| [\mathbf{D}_k^{\text{Rx}}]_{nq} \right| \cos \theta_{kq}^r \sin \phi_{kq}^r \sin(\xi_{knq}^{\text{Rx}}), \quad (40b)$$

$$\frac{\partial f_{\text{Quad}}}{\partial z_{kn}^r} = -\frac{4\pi}{\lambda} \sum_{k=1}^K \sum_{q=1}^{L_k^r} \left| [\mathbf{D}_k^{\text{Rx}}]_{nq} \right| \sin \theta_{kq}^r \sin(\xi_{knq}^{\text{Rx}}), \quad (40c)$$

respectively. The expressions of \mathbf{D}_k^{Rx} and ξ_{knq}^{Rx} are given by

$$\begin{aligned} \mathbf{D}_k^{\text{Rx}} &= \sqrt{\alpha_k} \bar{\mathbf{\Phi}}_k (\mathbf{I} + \bar{\mathbf{\Gamma}}_k) \bar{\mathbf{W}}_k^H \bar{\mathbf{G}}_k^H \Sigma_k^H \\ &- \bar{\mathbf{\Phi}}_k (\mathbf{I} + \bar{\mathbf{\Gamma}}_k) \bar{\mathbf{\Phi}}_k^H \mathbf{F}_k^H(\bar{\mathbf{R}}_k) \Sigma_k \bar{\mathbf{G}}_k \hat{\mathbf{W}}_k^H \Sigma_k^H. \quad (41) \end{aligned}$$

and

$$\begin{aligned} \xi_{knq}^{\text{Rx}} &= \angle [\mathbf{D}_k^{\text{Rx}}]_{nq} + \frac{2\pi}{\lambda} \left(x_{kn}^r \cos \theta_{kq}^r \cos \phi_{kq}^r \right. \\ &\quad \left. + y_{kn}^r \cos \theta_{kq}^r \sin \phi_{kq}^r + z_{kn}^r \sin \theta_{kq}^r \right), \quad (42) \end{aligned}$$

respectively, where we define $\bar{\mathbf{G}}_k \triangleq \mathbf{G}_k(\bar{\mathbf{T}})$. The closed-form expression of δ_k^{Rx} satisfying (39) is given by (43) at the bottom of the page. The derivations of (40) and (43) follow the same steps as (28) and (31), respectively. Hence, we omit them for brevity.

The global optimal solution of \mathbf{R}_k can be obtained in closed-form by assuming constraints (12d) and (37b) are inactive, given by

$$\mathbf{R}_k^* = \bar{\mathbf{R}}_k + \frac{1}{\delta_k^{\text{Rx}}} \nabla_{\mathbf{R}_k} f_{\text{Quad}}(\bar{\mathbf{R}}_k). \quad (44)$$

If \mathbf{R}_k^* does not satisfy constraint (12d) or (37b), we apply the interior-point method to obtain the optimal solution.

F. Box-Constrained Movement Mode for FAs

Although constraints (32) and (37b) are linear and compatible with quadratic optimization algorithms, they introduce $\frac{1}{2}M(M-1)$ and $\frac{1}{2}NK(N-1)$ inequalities, respectively. As the number of constraints grows proportionally to M^2 , solving problem (12) becomes infeasible for large M . Moreover, the original movement mode presents challenges for practical implementation. Since all FAs share a common movable region, mechanical conflicts may arise, limiting the feasibility of the design in real-world applications [37], [38].

Therefore, inspired by [23], [26], we propose a box-constrained movement mode for FAs. This approach ensures that constraints (12e) and (12f) are satisfied by maintaining a minimum gap D between neighboring boxes. With this movement mode, constraints (12e) and (12f) are incorporated into (12c) and (12d), respectively. Problems (21) and (36) are reformulated as

$$\max_{\mathbf{T}} f_{\text{Quad}}(\mathbf{T}) \quad \text{s. t. (12c)} \quad (45)$$

and

$$\max_{\mathbf{R}_k} f_{\text{Quad}}(\mathbf{R}_k) \quad \text{s. t. (12d),} \quad (46)$$

respectively. In problems (45) and (46), which consider the box-constrained movement mode, the total number of inequal-

$$\delta^{\text{Rx}} = \max_{1 \leq n \leq N} \frac{24\pi^2}{\lambda^2} L_k^r \left(\left(\sum_{j=1}^N \left| [\bar{\mathbf{\Phi}}_k]_n (\mathbf{I} + \bar{\mathbf{\Gamma}}_k) [\bar{\mathbf{\Phi}}_k]_j^H \right| + \sqrt{N} \left\| [\bar{\mathbf{\Phi}}_k]_n (\mathbf{I} + \bar{\mathbf{\Gamma}}_k) \bar{\mathbf{\Phi}}_k^H \right\|_2 \right) \left\| \Sigma_k \bar{\mathbf{G}}_k \hat{\mathbf{W}}_k^H \Sigma_k^H \right\|_2 + \sqrt{\frac{\alpha_k}{L_k^r}} \left\| [\bar{\mathbf{\Phi}}_k]_n (\mathbf{I} + \bar{\mathbf{\Gamma}}_k) \bar{\mathbf{W}}_k^H \bar{\mathbf{G}}_k^H \Sigma_k^H \right\|_2 \right). \quad (43)$$

ities in the constraints grows linearly with the number of FAs. Specifically, the numbers are M and NK , respectively.

Since problems (45) and (46) have only cuboid boundaries as constraints, the optimal solutions are obtained by projecting the unconstrained optima \mathbf{T}^* and \mathbf{R}_k^* onto the cuboid regions [23]. Thus, the closed-form solutions to problems (45) and (46) are given by

$$p_m^t = \min \left(\max \left(p_m^{t,*}, p_m^{\min} \right), p_m^{\max} \right), \quad (47a)$$

$$p_{kn}^r = \min \left(\max \left(p_{kn}^{r,*}, p_{kn}^{\min} \right), p_{kn}^{\max} \right), \quad (47b)$$

respectively, where p denotes a spatial coordinate, and can be replaced by x , y , or z , depending on the dimension being optimized. Specifically, $p_m^{t,*}$ and $p_{kn}^{r,*}$ are the entries of the unconstrained optimal solutions \mathbf{T}^* and \mathbf{R}_k^* , respectively.

The box-constrained movement mode restricts the feasible domain of the problem (12). Although this approach sacrifices some achievable WSR for reduced complexity, we will show in Section V-B that the degradation is negligible if the movable regions are sufficiently large. Based on the discussions above, we summarize the proposed BCA-based joint beamforming and antenna position optimization in Algorithm 1.

Algorithm 1 Overall BCA-based algorithm for solving (15)

Input: $M, N, K, P_{\max}, \alpha_k, \Sigma_k, L_k^t, L_k^r, \theta_{ki}^t, \phi_{ki}^t, \theta_{kj}^r, \phi_{kj}^r$.

- 1: Initialize \mathbf{W} , \mathbf{T} , and \mathbf{R} to corresponding feasible values.
- 2: **repeat**
- 3: Update each Φ_k via (17) and each Γ_k via (18).
- 4: Update each \mathbf{W}_k by bisection search via (20).
- 5: Update \mathbf{T} using MM according to Section III-D.
 - 5.1: Calculate δ^{Tx} via (31).
 - 5.2: **repeat**
 - 5.3: Calculate $\nabla_{\text{vec}(\mathbf{T})} f_{\text{Quad}}(\mathbf{T})$ via (28).
 - 5.4: Calculate \mathbf{T}^* via (34).
 - 5.5: Project \mathbf{T}^* onto cuboid regions via (47a).
 - 5.6: **until** the value of $f_{\text{Quad}}(\mathbf{T})$ converges.
- 6: Update \mathbf{R}_k using MM according to Section III-E.
 - 6.1: Calculate δ_k^{Rx} via (43).
 - 6.2: **repeat**
 - 6.3: Calculate $\nabla_{\text{vec}(\mathbf{R}_k)} f_{\text{Quad}}(\mathbf{R}_k)$ via (40).
 - 6.4: Calculate \mathbf{R}_k^* via (44).
 - 6.5: Project \mathbf{R}_k^* onto cuboid regions via (47b).
 - 6.6: **until** the value of $f_{\text{Quad}}(\mathbf{R}_k)$ converges.
- 7: **until** the value of R converges.

Output: \mathbf{W} , \mathbf{T} , \mathbf{R} .

IV. DECENTRALIZED IMPLEMENTATION OF THE BCA-BASED ALGORITHM

Although the proposed BCA-based algorithm in Section III can effectively solve the problem (12), its centralized implementation presents significant challenges as M increases. The reasons are summarized as follows.

- *Storage cost:* The CU requires substantial storage for CSI, beamforming matrices, and transmit FA positions, all of which have high dimensions.
- *Computational cost:* Matrix multiplications and inversions become increasingly prohibitive as M grows.
- *Interconnection cost:* In multiuser systems, antennas must transmit each user's CSI matrix to the CU, and the CU

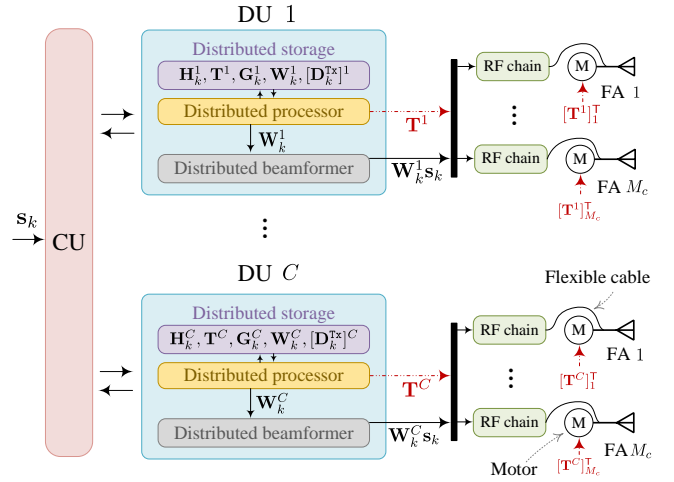


Fig. 2. DBP architecture for FA-assisted MU-MIMO systems.

must send the position information matrix to the FAs. Transmitting such high-dimensional matrices requires significant overhead.

To address the challenges while maintaining similar performance, we propose a decentralized implementation of Algorithm 1 based on the DBP architecture.

A. DBP Architecture

The DBP architecture is illustrated in Fig. 2, where the black solid line represents the data signal, and the red dash-dot line indicates the control signal. The DBP architecture is implemented on the BS side and partitions the transmit FA array into C clusters. Each cluster contains M_c transmit FAs with $M = CM_c$, and is managed by a DU with dedicated RF circuitry, storage, and a baseband processor. The black solid line represents the data signal, while the red dash-dot line indicates the control signal. With the DBP architecture, problem (12) is solved cooperatively by the CU and DUs, requiring data exchange between them. Specifically, the DUs compute the beamforming matrices \mathbf{W}_k and transmit FA positions \mathbf{T} , enabling both beamforming and FA position control at the DU.

Based on the DBP architecture, Algorithm 1 can be extended to its decentralized implementation that address the challenge above. Specifically, to alleviate the *storage cost*, any matrix of dimension M is stored distributively at the DUs. The superscript c denotes the submatrix stored across the c -th DU. Specifically, the variables requiring distributive storage include the channel matrix \mathbf{H}_k , the positions of transmit FAs \mathbf{T} , the FRMs for transmit FAs \mathbf{G}_k , the beamforming matrices \mathbf{W}_k , and the transpose of the first-order derivative of f_{Quad} w.r.t. \mathbf{G}_k , denoted as \mathbf{D}_k^{Tx} .

To manage the *computational cost*, we must ensure that complexity at both the CU and DUs is independent of M . In the remainder of this section, we discuss the distributed computation of each set of variables in the proposed BCA-based method. Besides, the low *interconnection cost* can be naturally achieved with reduced *storage cost*, as the dimensions of all stored matrices are independent of M .

B. Decentralized Calculation of \mathbf{M}_k , R , and f_{Quad}

The values of \mathbf{M}_k , R , and f_{Quad} , which are essential for evaluating system performance, are computed and stored at

the CU. To compute them, we define $\tilde{\mathbf{G}}_{kj} \triangleq \mathbf{G}_k(\mathbf{T})\mathbf{W}_j$ and compute $\tilde{\mathbf{G}}_{kj}$ distributively. To calculate $\tilde{\mathbf{G}}_{kj}$, each DU first computes $\mathbf{G}_k^c(\bar{\mathbf{T}}^c)\bar{\mathbf{W}}_j^c$ locally and then transmits the result to the CU. At the CU, $\tilde{\mathbf{G}}_{kj}$ is aggregated as

$$\tilde{\mathbf{G}}_{kj} = \sum_{c=1}^C \mathbf{G}_k^c(\bar{\mathbf{T}}^c)\bar{\mathbf{W}}_j^c. \quad (48)$$

Once the CU obtains $\tilde{\mathbf{G}}_{kj}$, the values of \mathbf{M}_k , R , and f_{Quad} are obtained by

$$\mathbf{M}_k = \sum_{j=1, j \neq k}^K \bar{\mathbf{F}}_k^H \Sigma_k \tilde{\mathbf{G}}_{kk} \tilde{\mathbf{G}}_{kk}^H \Sigma_k^H \bar{\mathbf{F}}_k + \sigma_k^2 \mathbf{I}, \quad (49)$$

$$R = \sum_{k=1}^K \alpha_k \log \det \left(\mathbf{I} + \bar{\mathbf{F}}_k^H \Sigma_k \tilde{\mathbf{G}}_{kk} \mathbf{M}_k^{-1} \tilde{\mathbf{G}}_{kk}^H \Sigma_k^H \bar{\mathbf{F}}_k + \sigma_k^2 \mathbf{I} \right), \quad (50)$$

and (51) at the bottom of the page, respectively.

C. Decentralized Update of $\underline{\Gamma}$ and $\underline{\Phi}$

The values of $\underline{\Gamma}$ and $\underline{\Phi}$ are computed and stored at the CU. Additionally, they can be transmitted to and stored at the DUs. Computing $\underline{\Gamma}$ and $\underline{\Phi}$ also requires $\tilde{\mathbf{G}}_{kj}$, which has already been calculated by (48). With $\tilde{\mathbf{G}}_{kj}$, the remaining computations for updating $\underline{\Gamma}$ and $\underline{\Phi}$ can be performed directly at the CU. The corresponding expressions are given by

$$\underline{\Gamma}_k = \tilde{\mathbf{G}}_{kk}^H \Sigma_k^H \bar{\mathbf{F}}_k \bar{\mathbf{M}}_k^{-1} \bar{\mathbf{F}}_k^H \Sigma_k \tilde{\mathbf{G}}_{kk}, \quad (52)$$

$$\underline{\Phi}_k = \sqrt{\alpha_k} \left(\bar{\mathbf{M}}_k + \bar{\mathbf{F}}_k^H \Sigma_k \tilde{\mathbf{G}}_{kk} \tilde{\mathbf{G}}_{kk}^H \Sigma_k^H \bar{\mathbf{F}}_k \right)^{-1} \bar{\mathbf{F}}_k^H \Sigma_k \tilde{\mathbf{G}}_{kk}. \quad (53)$$

D. The Decentralized Update of $\underline{\mathbf{W}}$

A major challenge in the decentralized update of $\underline{\mathbf{W}}$ is the matrix inversion in (20). Since matrix inversion of dimension M cannot be computed distributively, it is necessary to avoid matrix inversion in (20) to achieve a decentralized update of $\underline{\mathbf{W}}$. Therefore, we first discuss an inverse-free update step of $\underline{\mathbf{W}}$, followed by the proposed decentralized implementation of the algorithm.

If the quadratic term's coefficient matrix w.r.t. \mathbf{W}_k is diagonal, its inversion reduces to element-wise reciprocation of the diagonal entries, which can be computed distributively. Therefore, we introduce the following proposition to transform the coefficient matrix w.r.t. \mathbf{W}_k into a diagonal form.

Proposition 1 (Matrix non-homogeneous transform [30, Corollary 19]). *For Hermitian matrices \mathbf{L} and \mathbf{M} satisfying*

$\mathbf{M} \succeq \mathbf{L}$, the problem

$$\max_{\mathbf{X} \in \mathcal{X}} -\text{tr}(\mathbf{X}^H \mathbf{L} \mathbf{X}) \quad (54)$$

is equivalent to

$$\max_{\mathbf{X}, \mathbf{Z} \in \mathcal{X}} -\text{tr}(\mathbf{X}^H \mathbf{M} \mathbf{X} + 2\Re(\mathbf{X}^H (\mathbf{L} - \mathbf{M}) \mathbf{Z}) + \mathbf{Z}^H (\mathbf{M} - \mathbf{L}) \mathbf{Z}), \quad (55)$$

in the sense that they achieve identical optimal objective values with identical optimal solutions, where \mathbf{Z} is introduced as an auxiliary variable.

By applying Proposition 1 to $f_{\text{Quad}}(\underline{\mathbf{W}})$ and setting $\mathbf{M} = \eta \mathbf{I}$, where

$$\eta = \left\| \sum_{j=1}^K \bar{\mathbf{H}}_j^H \bar{\Phi}_j (\mathbf{I} + \bar{\Gamma}_j) \bar{\Phi}_j^H \bar{\mathbf{H}}_j \right\|_{\mathbb{F}}, \quad (56)$$

the problem (19) is reformulated as [30]

$$\max_{\underline{\mathbf{W}}, \underline{\Psi}} f_{\text{NonH}}(\underline{\mathbf{W}}, \underline{\Psi}) \quad \text{s. t. (12b)}, \quad (57)$$

where $f_{\text{NonH}}(\underline{\mathbf{W}}, \underline{\Psi})$ is given as (58) at the bottom of the page. For simplicity, we define $\underline{\Psi} = \{\Psi_k, \forall k\}$. Since the problem (57) involves both the auxiliary variables $\underline{\Psi}$ and the beamforming matrices $\underline{\mathbf{W}}$, we update one set of variables while keeping the other fixed.

First, we update $\underline{\Psi}$ while keeping $\underline{\mathbf{W}}$ fixed. According to Proposition 1, the optimal Ψ_k is given by

$$\Psi_k = \bar{\mathbf{W}}_k. \quad (59)$$

Next, we update $\underline{\mathbf{W}}$ while keeping $\underline{\Psi}$ fixed. By substituting (59) into (58) and setting the first-order derivative of $f_{\text{NonH}}(\underline{\mathbf{W}}, \bar{\mathbf{W}})$ w.r.t. \mathbf{W}_k to zero, we obtain the closed-form solution to the problem (57), given by

$$\mathbf{W}_k = \mathbf{Q}_k \min \left\{ \sqrt{\frac{P_{\max}}{\sum_{j=1}^K \text{tr}(\mathbf{Q}_j^H \mathbf{Q}_j)}}, 1 \right\}. \quad (60)$$

The matrix \mathbf{Q}_k denotes the beamforming matrix without the power constraint, and is given by

$$\mathbf{Q}_k = \frac{1}{\eta} \left(\sqrt{\alpha_k} \bar{\mathbf{H}}_k^H \bar{\Phi}_k (\mathbf{I} + \bar{\Gamma}_k) - \left(\sum_{j=1}^K \bar{\mathbf{H}}_j^H \bar{\Phi}_j (\mathbf{I} + \bar{\Gamma}_j) \bar{\Phi}_j^H \bar{\mathbf{H}}_j - \eta \mathbf{I} \right) \bar{\mathbf{W}}_k \right). \quad (61)$$

Although the per-iteration complexity is significantly reduced by eliminating matrix inversions, more iterations are required for convergence, which may still be time-consuming. Therefore, it is necessary to reduce the number of iterations.

As demonstrated in [31], we can reduce the number of iterations by using momentum methods. Among these methods, Nesterov's extrapolation strategy [39] extrapolates \mathbf{W}_k

$$f_{\text{Quad}}(\underline{\mathbf{W}}, \underline{\mathbf{T}}, \underline{\mathbf{R}}, \underline{\Gamma}, \underline{\Phi}) = \sum_{k=1}^K (\alpha_k \log \det(\mathbf{I} + \underline{\Gamma}_k) - \alpha_k \text{tr}(\underline{\Gamma}_k) + \text{tr} \left((\mathbf{I} + \underline{\Gamma}_k) \left(\sqrt{\alpha_k} \tilde{\mathbf{G}}_{kk}^H \Sigma_k^H \bar{\mathbf{F}}_k \underline{\Phi}_k + \sqrt{\alpha_k} \underline{\Phi}_k^H \bar{\mathbf{F}}_k^H \Sigma_k \tilde{\mathbf{G}}_{kk} - \underline{\Phi}_k^H \left(\sum_{j=1}^K \bar{\mathbf{F}}_k^H \Sigma_k \tilde{\mathbf{G}}_{kk} \tilde{\mathbf{G}}_{kk}^H \Sigma_k^H \bar{\mathbf{F}}_k + \sigma_k^2 \mathbf{I} \right) \underline{\Phi}_k \right) \right)). \quad (51)$$

$$f_{\text{NonH}}(\underline{\mathbf{W}}, \underline{\Psi}) = \sum_{k=1}^K \text{tr} \left(-\eta \mathbf{W}_k^H \mathbf{W}_k - 2\Re \left(\mathbf{W}_k^H \left(\sum_{j=1}^K \bar{\mathbf{H}}_j^H \bar{\Phi}_j (\mathbf{I} + \bar{\Gamma}_j) \bar{\Phi}_j^H \bar{\mathbf{H}}_j - \eta \mathbf{I} \right) \Psi_k \right) - \Psi_k^H \left(\eta \mathbf{I} - \sum_{j=1}^K \bar{\mathbf{H}}_j^H \bar{\Phi}_j (\mathbf{I} + \bar{\Gamma}_j) \bar{\Phi}_j^H \bar{\mathbf{H}}_j \right) \Psi_k + (\mathbf{I} + \underline{\Gamma}_k) (\sqrt{\alpha_k} \mathbf{W}_k^H \bar{\mathbf{H}}_k^H \bar{\Phi}_k + \sqrt{\alpha_k} \bar{\Phi}_k^H \bar{\mathbf{H}}_k \mathbf{W}_k) \right) + \text{const.} \quad (58)$$

along the direction defined by the two previous iterations, $\overline{\mathbf{W}}_k$ and $\overline{\overline{\mathbf{W}}}_k$, to predict its value in the following iteration. This approach has been shown to be effective in this scenario [31]. The extrapolated value Υ_k is defined as

$$\Upsilon_k \triangleq \overline{\mathbf{W}}_k + \nu_i \left(\overline{\mathbf{W}}_k - \overline{\overline{\mathbf{W}}}_k \right). \quad (62)$$

where ν_i denotes the extrapolation step size in the i -th BCA iteration, and is given by

$$\nu_i = \max \left\{ \frac{i-2}{i+1}, 0 \right\}. \quad (63)$$

Using Nesterov's extrapolation strategy, the matrix \mathbf{Q}_k is calculated as

$$\mathbf{Q}_k = \eta^{-1} \left(\sqrt{\alpha_k} \overline{\mathbf{H}}_k^H \overline{\mathbf{F}}_k (\mathbf{I} + \overline{\mathbf{\Gamma}}_k) - \left(\sum_{j=1}^K \overline{\mathbf{H}}_j^H \overline{\mathbf{F}}_j (\mathbf{I} + \overline{\mathbf{\Gamma}}_j) \overline{\mathbf{F}}_j^H \overline{\mathbf{H}}_j - \eta \mathbf{I} \right) \Upsilon_k \right). \quad (64)$$

Then, the matrix \mathbf{W}_k is obtained by substituting (64) into (60).

After obtaining the improved closed-form expression of $\overline{\mathbf{W}}$ given in (60) and (64), the decentralized update of $\overline{\mathbf{W}}$ can be achieved correspondingly. First, we compute η distributively. By leveraging the positive semi-definiteness of the matrix $\mathbf{I} + \overline{\mathbf{\Gamma}}_k$, we can decompose it by

$$\mathbf{I} + \overline{\mathbf{\Gamma}}_k = \overline{\mathbf{\Xi}}_k \sqrt{\Lambda_k} \sqrt{\Lambda_k^T \overline{\mathbf{\Xi}}_k^H}, \quad (65)$$

where $\Lambda_k \in \mathbb{R}_+^{d \times d}$ is a diagonal matrix of eigenvalues, and $\overline{\mathbf{\Xi}}_k \in \mathbb{C}^{d \times d}$ contains the corresponding eigenvectors. Therefore, η can be calculated using the trace property of the Frobenius norm, given by

$$\eta = \sqrt{\sum_{j=1}^K \sum_{k=1}^K \text{tr}(\mathbf{P}_k^H \mathbf{P}_j \mathbf{P}_k^H \mathbf{P}_j)}, \quad (66)$$

where we define $\mathbf{P}_k \triangleq \overline{\mathbf{H}}_k^H \overline{\mathbf{F}}_k \overline{\mathbf{\Xi}}_k \sqrt{\Lambda_k}$, and it is distributively computed at the DUs. Specifically, CU broadcasts Λ_k and $\overline{\mathbf{\Xi}}_k$ to all DUs, and each DU first computes \mathbf{P}_k^c as

$$\mathbf{P}_k^c \triangleq \left(\overline{\mathbf{H}}_k^c \right)^H \overline{\mathbf{F}}_k \overline{\mathbf{\Xi}}_k \sqrt{\Lambda_k}. \quad (67)$$

Then, each DU computes $(\mathbf{P}_k^c)^H \mathbf{P}_j^c$ locally and transmits the result to the CU. Finally, the CU aggregates the results as $\tilde{\mathbf{P}}_{kj} = \sum_{c=1}^C (\mathbf{P}_k^c)^H \mathbf{P}_j^c$, and computes η as

$$\eta = \sqrt{\sum_{j=1}^K \sum_{k=1}^K \text{tr}(\tilde{\mathbf{P}}_{kj} \tilde{\mathbf{P}}_{kj})}. \quad (68)$$

Note that (68) is equivalent to (66) since $\tilde{\mathbf{P}}_{kj} = \mathbf{P}_k^H \mathbf{P}_j$.

Next, we use the previously computed η to calculate \mathbf{W}_k^c , which is stored distributively at each DU. First, we compute the extrapolated beamforming matrices Υ_k , which is stored distributively. At the c -th DU, the matrix Υ_k^c is computed as

$$\Upsilon_k^c = \overline{\mathbf{W}}_k^c + \nu_i \left(\overline{\mathbf{W}}_k^c - \overline{\overline{\mathbf{W}}}_k^c \right). \quad (69)$$

Then, we compute \mathbf{Q}_k , which is also stored distributively as \mathbf{Q}_k^c . After each DU locally computes $\overline{\mathbf{H}}_j^c \Upsilon_k^c$ and transmits the result to the CU, the CU aggregates the received $\overline{\mathbf{H}}_j^c \Upsilon_k^c$ to obtain $\tilde{\Upsilon}_{jk}$ as

$$\tilde{\Upsilon}_{jk} = \sum_{c=1}^C \overline{\mathbf{H}}_j^c \Upsilon_k^c, \quad (70)$$

and broadcasts the result $\tilde{\Upsilon}_{jk}$ to each DU. Therefore, the calculation of \mathbf{Q}_k^c is given by

$$\mathbf{Q}_k^c = \eta^{-1} \sqrt{\alpha_k} \left(\overline{\mathbf{H}}_k^c \right)^H \overline{\mathbf{F}}_k (\mathbf{I} + \overline{\mathbf{\Gamma}}_k) - \eta^{-1} \sum_{j=1}^K \left(\overline{\mathbf{H}}_j^c \right)^H \overline{\mathbf{F}}_j (\mathbf{I} + \overline{\mathbf{\Gamma}}_j) \overline{\mathbf{F}}_j^H \tilde{\Upsilon}_{jk} + \Upsilon_k^c. \quad (71)$$

Finally, we compute \mathbf{W}_k^c based on \mathbf{Q}_k^c . We define $\text{tr}(\tilde{\mathbf{Q}}_k) \triangleq \text{tr}(\mathbf{Q}_k^H \mathbf{Q}_k)$ and compute them distributively. Specifically, each DU locally computes $\text{tr}((\mathbf{Q}_k^c)^H \mathbf{Q}_k^c)$ and transmits the result to the CU. The CU then aggregates the received values to compute $\text{tr}(\tilde{\mathbf{Q}}_k)$ as

$$\text{tr}(\tilde{\mathbf{Q}}_k) = \sum_{c=1}^C \text{tr}((\mathbf{Q}_k^c)^H \mathbf{Q}_k^c). \quad (72)$$

Once $\text{tr}(\tilde{\mathbf{Q}}_k)$ is obtained, it will be broadcasted to all DUs. Finally, \mathbf{W}_k^c can be computed at the c -th DU as

$$\mathbf{W}_k^c = \mathbf{Q}_k^c \min \left\{ \sqrt{\frac{P_{\max}}{\sum_{j=1}^K \text{tr}(\tilde{\mathbf{Q}}_j)}}, 1 \right\}. \quad (73)$$

E. Decentralized Update of \mathbf{T} and \mathbf{R}

To update \mathbf{T} and \mathbf{R} distributively, we must compute \mathbf{D}_k^{Tx} , \mathbf{D}_k^{Rx} , δ_k^{Tx} , and δ_k^{Rx} distributively in advance. The matrix \mathbf{D}_k^{Tx} is stored distributively as $[\mathbf{D}_k^{\text{Tx}}]^c$, whereas \mathbf{D}_k^{Rx} is stored at the CU. To calculate \mathbf{D}_k^{Tx} , the CU broadcasts $\overline{\mathbf{\Gamma}}_k$, $\overline{\mathbf{F}}_k$, and $\tilde{\mathbf{G}}_{kj}$ to each DU. Then, the c -th DU computes $[\mathbf{D}_k^{\text{Tx}}]^c$ as

$$[\mathbf{D}_k^{\text{Tx}}]^c = \sqrt{\alpha_k} \overline{\mathbf{W}}_k^c (\mathbf{I} + \overline{\mathbf{\Gamma}}_k) \overline{\mathbf{F}}_k^H \Sigma_k - \sum_{j=1}^K \overline{\mathbf{W}}_j^c \tilde{\mathbf{G}}_{kj}^H \Sigma_k^H \overline{\mathbf{F}}_k \overline{\mathbf{F}}_k^H (\mathbf{I} + \overline{\mathbf{\Gamma}}_k) \overline{\mathbf{F}}_k^H \overline{\mathbf{F}}_k \Sigma_k. \quad (74)$$

Meanwhile, as indicated by (41), calculating \mathbf{D}_k^{Rx} requires only $\tilde{\mathbf{G}}_{kj}$, which has been computed using (48). The remaining calculations in (41) are performed at the CU, given by

$$\mathbf{D}_k^{\text{Rx}} = \sqrt{\alpha_k} \overline{\mathbf{F}}_k (\mathbf{I} + \overline{\mathbf{\Gamma}}_k) \tilde{\mathbf{G}}_{kj}^H \Sigma_k^H - \overline{\mathbf{F}}_k (\mathbf{I} + \overline{\mathbf{\Gamma}}_k) \overline{\mathbf{F}}_k^H \overline{\mathbf{F}}_k \Sigma_k \sum_{j=1}^K \tilde{\mathbf{G}}_{kj} \tilde{\mathbf{G}}_{kj}^H \Sigma_k^H. \quad (75)$$

Scalars δ_k^{Tx} and δ_k^{Rx} are stored at the CU. To compute the values distributively, we define $\tilde{\mathbf{W}}_{kj} \triangleq \overline{\mathbf{W}}_k^H \overline{\mathbf{W}}_j$ and compute $\tilde{\mathbf{W}}_{kj}$ distributively. First, each DU computes $(\overline{\mathbf{W}}_k^c)^H \overline{\mathbf{W}}_j^c$ and

$$\delta_k^{\text{Tx}} = \max_{1 \leq m \leq M} \frac{24\pi^2}{\lambda^2} \sum_{k=1}^K L_k^t \left(\left(\sum_{t=1}^K \|\overline{\mathbf{W}}_t^c\|_2 \sum_{j=1}^M \|\overline{\mathbf{W}}_t\|_2 + \sum_{t=1}^K \sum_{s=1}^K \|\overline{\mathbf{W}}_t^c\|_2 \|\overline{\mathbf{W}}_s^c\|_2 \right) \times \|\Sigma_k^H \overline{\mathbf{F}}_k \overline{\mathbf{F}}_k (\mathbf{I} + \overline{\mathbf{\Gamma}}_k) \overline{\mathbf{F}}_k^H \overline{\mathbf{F}}_k \Sigma_k\|_2 + \sqrt{\frac{\alpha_k}{L_k^t}} \|\overline{\mathbf{W}}_k^c\|_2 \|\overline{\mathbf{F}}_k (\mathbf{I} + \overline{\mathbf{\Gamma}}_k) \overline{\mathbf{F}}_k^H \overline{\mathbf{F}}_k \Sigma_k\|_2 \right). \quad (78)$$

$$\delta_k^{\text{Rx}} = \max_{1 \leq n \leq N} \frac{24\pi^2}{\lambda^2} L_k^r \left(\left(\sum_{j=1}^N \|\overline{\mathbf{F}}_k\|_2 \|\overline{\mathbf{F}}_j\|_2 + \sqrt{N} \|\overline{\mathbf{F}}_k\|_2 \|\overline{\mathbf{F}}_k\|_2 \right) \times \left\| \sum_{t=1}^K \Sigma_k \tilde{\mathbf{G}}_{kt} \tilde{\mathbf{G}}_{kt}^H \Sigma_k^H \right\|_2 + \sqrt{\frac{\alpha_k}{L_k^r}} \|\overline{\mathbf{F}}_k\|_2 \|\overline{\mathbf{F}}_k (\mathbf{I} + \overline{\mathbf{\Gamma}}_k) \tilde{\mathbf{G}}_{kk}^H \Sigma_k^H\|_2 \right). \quad (79)$$

transmits the result to the CU, where $\tilde{\mathbf{W}}_{kj}$ is aggregated as

$$\tilde{\mathbf{W}}_{kj} = \sum_{c=1}^C \left(\overline{\mathbf{W}}_k^c \right)^H \overline{\mathbf{W}}_j^c. \quad (76)$$

However, δ^{Tx} still cannot be computed distributively since $\hat{\mathbf{W}}$ in (31) cannot be stored and calculated. Therefore, we apply the triangle inequality and Cauchy-Schwarz inequality to $\sum_{j=1}^M |[\hat{\mathbf{W}}]_{mj}|$ and obtain

$$\sum_{j=1}^M |[\hat{\mathbf{W}}]_{mj}| \leq \sum_{k=1}^K \left\| \left[\overline{\mathbf{W}}_k^c \right]_m \right\|_2 \sum_{c'=1}^C \sum_{j=1}^{M_c} \left\| \left[\overline{\mathbf{W}}_k^{c'} \right]_j \right\|_2. \quad (77)$$

To calculate the r.h.s. of (77), each DU first computes $\sum_{j=1}^{M_c} \left\| \left[\overline{\mathbf{W}}_k^c \right]_j \right\|_2$ and transmits it to the CU. Then, the CU calculates the summation $\sum_{c=1}^C \sum_{j=1}^{M_c} \left\| \left[\overline{\mathbf{W}}_k^c \right]_j \right\|_2$ and broadcasts it back to DUs, where the r.h.s. of (77) is finally computed.

Plugging (76) and (77) into (31), we obtain the expression for computing δ^{Tx} , given by (78) at the bottom of the previous page. To compute δ^{Tx} distributively as in (78), the CU first broadcasts $\tilde{\mathbf{W}}_{kj}$ to all DUs. Then, each DU computes the argument of the maximization operation in (31) and selects the greatest value to send to the CU. After receiving C values from the DUs, the CU determines the largest value, and set it as δ^{Tx} . The expression for δ_k^{Rx} is obtain by plugging (76) into (43), and it is given by (79) at the bottom of the previous page. The value of δ_k^{Rx} is computed directly at the CU.

Once the values of \mathbf{D}_k^{Tx} , \mathbf{D}_k^{Rx} , δ^{Tx} , and δ_k^{Rx} are obtained, the surrogate functions in (27) and (38) can be computed accordingly. To update \mathbf{T} , the CU first broadcasts δ^{Tx} to all DUs. Each DU then computes the closed-form unconstrained global optimum $[\mathbf{T}^*]^c$ as

$$[\mathbf{T}^*]^c = \overline{\mathbf{T}}^c + \frac{1}{\delta^{\text{Tx}}} \nabla_{\mathbf{T}^c} f_{\text{Quad}}(\overline{\mathbf{T}}), \quad (80)$$

where the entries of $\nabla_{\mathbf{T}^c} f_{\text{Quad}}(\overline{\mathbf{T}})$ are computed at the DU using (28), with \mathbf{D}_k^{Tx} replaced by $[\mathbf{D}_k^{\text{Tx}}]^c$. Once $[\mathbf{T}^*]^c$ is obtained, the DU updates \mathbf{T}^c by projecting $[\mathbf{T}^*]^c$ onto the cuboid region using (47a). Moreover, the CU updates \mathbf{R} as described in (44) and (47b). To summarize, the key processes of the above decentralized implementation of Algorithm 1 are presented in Algorithm 2.

Algorithm 2 Decentralized Implementation of Algorithm 1

Input: $C, M, N, K, P_{\max}, \alpha_k, \Sigma_k, L_k^t, L_k^r, \theta_{ki}^t, \phi_{ki}^t, \theta_{kj}^r, \phi_{kj}^r$.

- 1: Initialize $\underline{\mathbf{W}}$, \mathbf{T} , and $\underline{\mathbf{R}}$ to corresponding feasible values.
- 2: **repeat**
- 3: Update each Φ_k and Γ_k distributively according to the steps in Section IV-C and store the results at the CU.
- 4: Update each $[\mathbf{W}_k]^c$ distributively according to the steps in Section IV-D and store it at the c -th DU.
- 5: Update $[\mathbf{T}]^c$ and \mathbf{R}_k distributively according to the steps in Section IV-E, and store them at the c -th DU and the CU, respectively.
- 6: **until** the value of R converges.

Output: $[\mathbf{W}_k]^c, [\mathbf{T}]^c, \mathbf{R}_k$.

F. Complexity Analysis

For the centralized implementation given in Algorithm 1, the time complexity of a single BCA iteration is dominated by the updates of $\underline{\mathbf{W}}$ and \mathbf{T} , and is given by $\mathcal{O}(M^3 T_{\text{bis}} + M^2 L_k^t T_{\text{MM}}^{\text{Tx}})$. Here, T_{bis} denotes the number of iterations in the

bisection search for updating \mathbf{W} described in Section III-C, and $T_{\text{MM}}^{\text{Tx}}$ represents the average number of MM iterations required for updating \mathbf{T} . The complexity of the centralized implementation is proportional to M^3 and grows rapidly as the number of transmit FAs M increases.

In comparison, the complexity of the decentralized implementation at the CU is given by $\mathcal{O}(K^2 d^3 + N^3 K + T_{\text{MM}}^{\text{Rx}}(N^2 L_k^r + N(L_k^r)^2))$, and the complexity at each DU is given by $\mathcal{O}(NK^2 d + K^2 d^2 + T_{\text{MM}}^{\text{Tx}}(M_c d L_k^t + d(L_k^t)^2))$, where $T_{\text{MM}}^{\text{Tx}}$ and $T_{\text{MM}}^{\text{Rx}}$ represent the MM iterations for the update step of \mathbf{T} and \mathbf{R} , respectively. Notably, the complexities of the CU and each DU are independent of M and are significantly lower than that of the centralized implementation.

V. SIMULATION

In this section, we evaluate the performance of FA-assisted MU-MIMO networks optimized using the proposed centralized BCA-based algorithm in Algorithm 1 and its decentralized implementation in Algorithm 2, denoted as ‘‘C’’ and ‘‘D’’, respectively.

We denote the system with joint beamforming and transmit and receive FA position optimization as transmit and receive FA (TRFA), which is optimized by our algorithms. We compare the performance of TRFA with several baselines, specified as follows.

- 1) **FPA:** The antenna arrays at the BS and users are fixed in position with a spacing of $\lambda/2$. The update steps for \mathbf{T} and \mathbf{R} are skipped.
- 2) **Random-position antenna (RPA):** The antennas at the BS and the users are FAs with random positions.
- 3) **Transmit FA (TFA):** The antennas at the users are fixed with a spacing of $\lambda/2$, while the antennas at the BS are FAs. The update step for \mathbf{R} is skipped.
- 4) **Receive FA (RFA):** The antennas at the BS are fixed with a spacing of $\lambda/2$, while the antennas at the users are FAs. The update step for \mathbf{T} is skipped.

A. Simulation Setup

We consider a downlink MU-MIMO system with $K = 6$ users, each equipped with $N = 4$ FAs. The number of parallel data streams is set to $d = 4$. All users have equal priority, given by $\alpha_k = 1$. The system operates over a millimeter-wave channel with a carrier frequency of $f_c = 28$ GHz [37]. Unless otherwise specified, the power budget is set to $P_{\max} = 20$ dBm. The users are uniformly distributed within an annular region centered at the BS. Consequently, the distance between the BS and each UE d_k follows the distribution $d_k^2 \sim \mathcal{U}[d_{\min}^2, d_{\max}^2]$, where $d_{\min} = 20$ m and $d_{\max} = 100$ m. The pathloss is modeled as $\kappa(d_k) = T_0 \left(\frac{d_k}{d_0}\right)^{-\varrho}$, where the reference pathloss at $d_0 = 1$ m is $T_0 = 20 \lg(4\pi d_0/\lambda) = 61.4$ dB, and the pathloss exponent is $\varrho = 3.67$ [30], [31]. The elevation and azimuth AoAs and AoDs are assumed to follow uniform distributions, i.e., $\theta_{ki}^t \sim \mathcal{U}[0, \pi]$, $\phi_{ki}^t \sim \mathcal{U}[0, \pi]$, $\theta_{kj}^r \sim \mathcal{U}[0, \pi]$, and $\phi_{kj}^r \sim \mathcal{U}[0, \pi]$. The number of transmit and receive paths between the BS and user k is assumed identical, i.e., $L_k^t = L_k^r = 3$ [37]. Consequently, the PRM matrices Σ_k are square and assumed diagonal, with elements distributed as $[\Sigma_k]_{qq} \sim \mathcal{CN}(0, (\kappa(d_k)L)^{-1})$ [25]. Unless otherwise specified, the simulation results are averaged over 200 independent channel realizations.

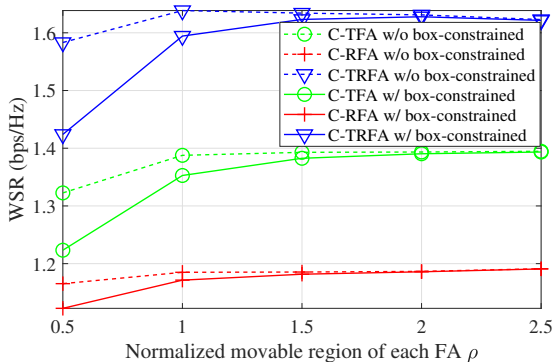


Fig. 3. WSR comparison with and without the box-constrained movement mode.

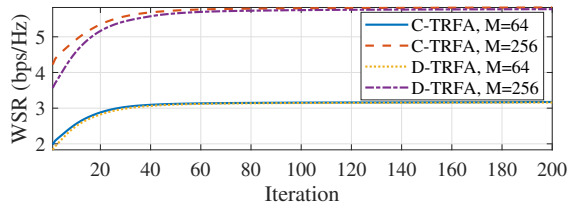


Fig. 4. Convergence behavior of the proposed algorithms.

The minimal distance between any pair of FAs is set as $D = \lambda/2$. Let ρ denote the movable region of each antenna, normalized by λ . Without the box-constrained movement mode, all transmit (and receive) FAs can move within a shared cuboid region, where the edge length is $\rho\lambda\sqrt{M}$ (and $\rho\lambda\sqrt{N}$), and the height is $2\rho\lambda$. With the box-constrained movement mode, the specific movable regions of each FA are detailed in Section III-F.

B. Impact of Box-Constrained Movement Mode

We evaluate the impact of the box-constrained movement mode on system performance. The parameter ρ is used to control the size of the movable region for each FA. Specifically, when $\rho = 0.5$, each FA is restricted to movement along the y -axis for the box-constrained movement mode. As ρ increases, the movable region expands, allowing greater flexibility.

Fig. 3 presents the simulation results, which is averaged over 10^3 samples with $M = 16$. The WSR performance gap between systems with and without the box-constrained movement mode decreases as ρ increases. Notably, when $\rho \geq 2$, the performance gap remains below 0.3%. This indicates that when the movable region of each FA is sufficiently large, the impact of the box-constrained movement mode on performance is negligible. This is because a larger movable region for each FA increases the likelihood of avoiding deep fading channels. Based on this observation, we only test the performance with the box-constrained movement mode, and set $\rho = 2$ for all subsequent simulations.

C. Convergence Behavior

Fig. 4 illustrates the convergence behavior of our proposed algorithms. Regardless of the number of transmit FAs M , all algorithms converge within 80 iterations. Moreover, all curves increase with the number of iterations, confirming the convergence of our proposed algorithms.

The decentralized implementation experiences a slight performance loss compared with the centralized approach, especially in the initial iterations. However, the total number of

TABLE I
WSR PERFORMANCE COMPARISON

M	P_{\max} (dBm)	WSR (bps/Hz)				
		FPA	RPA	TFA	RFA	TRFA (ours)
16	20	0.864	0.830	1.30	1.11	1.55
	30	3.30	3.28	4.15	3.89	4.62
64	20	2.12	2.07	2.78	2.38	3.11
	30	6.68	6.81	7.69	7.26	8.27
256	20	4.30	4.31	5.18	4.67	5.62
	30	12.8	13.2	13.7	13.6	14.5

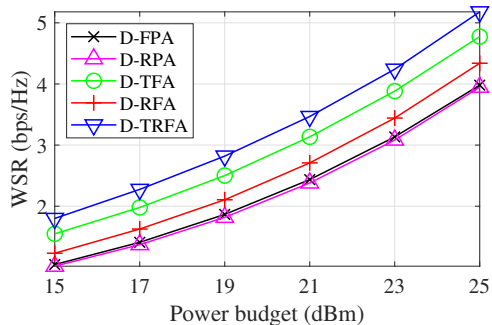


Fig. 5. WSR versus the power budget P_{\max} .

iterations required for convergence remains similar. Moreover, the performance gap is less than 1% after convergence, making the difference negligible. Therefore, we evaluate only the decentralized implementation for all subsequent simulations.

D. Performance Comparison

We compare the WSR of TRFA optimized by the decentralized implementation of our proposed algorithm with several baselines under different configurations, as shown in Table I. The performance of TRFA is consistently the highest across all configurations, demonstrating its superior performance. Specifically, a larger transmit FA number M and a higher power budget P_{\max} lead to a significant absolute WSR increase. Meanwhile, when the transmit FA number M is smaller and the power budget P_{\max} is lower, the relative WSR improvement over FPA is more pronounced. With $M = 64$ and $P_{\max} = 20$ dBm, the WSR increases by approximately 47%. For $M = 256$ and $P_{\max} = 30$ dBm, the WSR gain over FPA is about 1.7 bps/Hz.

The effectiveness of our proposed optimization algorithm is further validated by comparing the WSR values of TRFA and RPA. The WSR of RPA is similar to that of FPA, indicating that random FA position adjustments hardly provide any performance gain. In contrast, TRFA achieves significantly higher WSR than FPA, demonstrating that our algorithm effectively optimizes FA positions to enhance performance.

E. Impact of Power Budget and Number of Users

Fig. 5 illustrates the WSR performance with different transmit power budgets, where we set $M = 64$. The WSR of all systems increases significantly with a higher transmit power budget, and TRFA consistently outperforms the baselines. This is because the FA can dynamically reconstruct the channel, improving the receive SINR with the same transmit power. Therefore, utilizing FA can significantly reduce the required transmit power. Specifically, by fixing the WSR at 2 bps/Hz, the transmit power budget can be reduced by over 3 dB, demonstrating the superior performance of the FA-assisted MU-MIMO system.

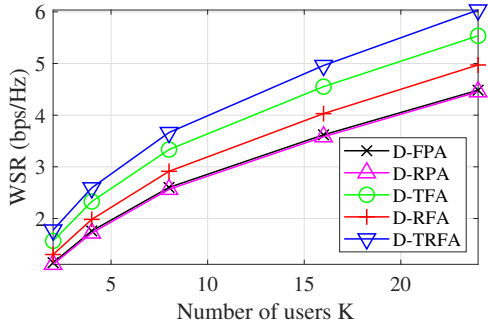


Fig. 6. WSR versus the number of users K .

TABLE II
CPU TIME SAVED COMPARED WITH CENTRALIZED
IMPLEMENTATION (%)

M	C	FPA	TFA	RFA	TRFA
64	4	89.6%	64.5%	89.3%	69.4%
	16	98.3%	89.4%	90.4%	87.9%
256	4	99.2%	68.6%	97.8%	71.9%
	16	99.5%	80.5%	97.8%	82.4%

Meanwhile, the impact of the number of users is shown in Fig. 6 for $M = 64$. The WSR of TRFA consistently exceeds that of all baselines, demonstrating its superior performance in multiuser systems. More importantly, as the number of users K increases, the performance gap between TRFA and the baselines widens. With more users, conventional MU-MIMO systems with FPAs experience stronger MUI. In contrast, FAs can be dynamically repositioned to mitigate MUI, thereby enhancing system capacity.

F. Computational Efficiency of Decentralized Implementation

We assess the computational efficiency of the proposed decentralized implementation by measuring the central processing unit (CPU) time of each algorithm. Specifically, for centralized implementations, the total CPU time is recorded. For decentralized implementations, the CPU time is calculated as the sum of the CU's CPU time and the maximum running time among all DUs.

The results in Table II show that decentralized implementations significantly reduce computation time compared with centralized implementations across all system configurations. The proposed decentralized approach demonstrates high computational efficiency, achieving at least a 69.4% reduction in CPU time. This improvement is attributed to the parallel processing capability of DUs, where each DU independently solves a smaller-scale problem. As the number of DUs C increases, the problem size of each DU decreases, leading

to greater parallelism. Consequently, for a fixed number of transmit FAs M , the CPU time reduction becomes more pronounced. However, increasing the number of DUs also introduces higher hardware complexity and interconnection costs, highlighting a tradeoff between computational efficiency and system complexity.

VI. CONCLUSION

In this paper, we considered the joint beamforming and antenna position optimization for WSR maximization in FA-assisted MU-MIMO systems. We decoupled the original WSR maximization problem using matrix FP techniques and employed BCA to solve the resulting subproblems. To optimize FA positions, we proposed a novel MM algorithm capable of optimizing all antenna positions simultaneously. To further reduce computational, storage, and interconnection costs, we proposed a decentralized implementation of our algorithm based on the DBP architecture. Simulation results demonstrated that FA-assisted MU-MIMO networks optimized by our algorithms achieve significant performance gains across various setups. Moreover, the decentralized implementation substantially improves computational efficiency.

APPENDIX

A. Derivation of $\nabla_{\text{vec}(\mathbf{T})} f_{\text{Quad}}(\mathbf{T})$ and δ^{Tx}

Using the chain rule, we compute the entries of $\nabla_{\text{vec}(\mathbf{T})} f_{\text{Quad}}(\mathbf{T})$ via (81) at the bottom of the page, where the calculation of $\frac{\partial f_{\text{Quad}}}{\partial \mathbf{G}_k}$ and $\frac{\partial \mathbf{G}_k}{\partial p_m^t}$ are given by (29) and

$$\frac{\partial \mathbf{G}_k}{\partial p_m^t} = \left[\mathbf{0}, \dots, \mathbf{0}, \frac{\partial \mathbf{g}_k(\mathbf{t}_m)}{\partial p_m^t}, \mathbf{0}, \dots, \mathbf{0} \right], \quad (82)$$

respectively. Here, the q -th entries of $\frac{\partial \mathbf{g}_k(\mathbf{t}_m)}{\partial p_m^t}$, $p \in \{x, y, z\}$, is given by (83) at the bottom of the page. Plugging (29) and (82) into (81), we obtain the expression of $\nabla_{\text{vec}(\mathbf{T})} f_{\text{Quad}}(\mathbf{T})$.

We utilize the inequality (26) to derive the closed-form expression for δ^{Tx} . Specifically, we approximate the maximum eigenvalue of the Hessian matrix $\nabla_{\text{vec}(\mathbf{T})}^2 f_{\text{Quad}}(\mathbf{T})$ using an upper bound on its matrix infinity norm [40]. To compute this upper bound, we first determine the maximum absolute value of each entry in the Hessian matrix. The absolute values of these entries are given by (84a) at the top of the next page. Next, we derive an upper bound on $\|[\mathbf{D}_k^{\text{Tx}}]\|_2$ for any \mathbf{T} , which provides an upper bound for (84a). The resulting upper bound on $\|[\mathbf{D}_k^{\text{Tx}}]\|_2$ is given by (85) at the top of the next page. By substituting (85) into (84a), we derive the upper bounds of the absolute values of the entries in $\nabla_{\text{vec}(\mathbf{T})}^2 f_{\text{Quad}}(\mathbf{T})$, given by (84b) at the top of the next page. For simplicity, we define the upper bounds of $|\frac{\partial^2 f_{\text{Quad}}}{\partial p_m^t \partial p_j^t}|$ as γ_{mj}^{Tx} . Finally, the upper bound

$$\frac{\partial f_{\text{Quad}}}{\partial p_m^t} = \sum_{k=1}^K \text{tr} \left(\left(\frac{\partial f_{\text{Quad}}}{\partial \mathbf{G}_k} \right)^{\text{T}} \frac{\partial \mathbf{G}_k}{\partial p_m^t} + \frac{\partial \mathbf{G}_k^{\text{H}}}{\partial p_m^t} \left(\frac{\partial f_{\text{Quad}}}{\partial \mathbf{G}_k^{\text{H}}} \right)^{\text{T}} \right) = 2 \sum_{k=1}^K \Re \left\{ \text{tr} \left(\left(\frac{\partial f_{\text{Quad}}}{\partial \mathbf{G}_k} \right)^{\text{T}} \frac{\partial \mathbf{G}_k}{\partial p_m^t} \right) \right\} \quad (81)$$

$$\left[\frac{\partial \mathbf{g}_k(\mathbf{t}_m)}{\partial x_m^t} \right]_q = j \frac{2\pi}{\lambda} \cos \theta_{kq}^t \cos \phi_{kq}^t \exp \left[j \frac{2\pi}{\lambda} (x_m^t \cos \theta_{kq}^t \cos \phi_{kq}^t + y_m^t \cos \theta_{kq}^t \sin \phi_{kq}^t + z_m^t \sin \theta_{kq}^t) \right], \quad (83a)$$

$$\left[\frac{\partial \mathbf{g}_k(\mathbf{t}_m)}{\partial y_m^t} \right]_q = j \frac{2\pi}{\lambda} \cos \theta_{kq}^t \sin \phi_{kq}^t \exp \left[j \frac{2\pi}{\lambda} (x_m^t \cos \theta_{kq}^t \cos \phi_{kq}^t + y_m^t \cos \theta_{kq}^t \sin \phi_{kq}^t + z_m^t \sin \theta_{kq}^t) \right], \quad (83b)$$

$$\left[\frac{\partial \mathbf{g}_k(\mathbf{t}_m)}{\partial z_m^t} \right]_q = j \frac{2\pi}{\lambda} \sin \theta_{kq}^t \exp \left[j \frac{2\pi}{\lambda} (x_m^t \cos \theta_{kq}^t \cos \phi_{kq}^t + y_m^t \cos \theta_{kq}^t \sin \phi_{kq}^t + z_m^t \sin \theta_{kq}^t) \right]. \quad (83c)$$

$$\left| \frac{\partial^2 f_{\text{Quad}}}{\partial p_m^t \partial p_j^t} \right| = 2 \left| \sum_{k=1}^K \Re \left\{ -[\hat{\mathbf{W}}]_{mj} \left(\frac{\partial \mathbf{g}_k^H(\mathbf{t}_j)}{\partial p_j^t} \right)^H \boldsymbol{\Sigma}_k^H \bar{\mathbf{F}}_k \bar{\boldsymbol{\Phi}}_k (\mathbf{I} + \bar{\boldsymbol{\Gamma}}_k) \bar{\boldsymbol{\Phi}}_k^H \bar{\mathbf{F}}_k^H \boldsymbol{\Sigma}_k \left(\frac{\partial \mathbf{g}_k(\mathbf{t}_m)}{\partial p_m^t} \right) + \delta_{mj} [\mathbf{D}_k^{\text{Tx}}]_m \frac{\partial^2 \mathbf{g}_k(\mathbf{t}_m)}{\partial p_m^t \partial p_j^t} \right\} \right| \quad (84a)$$

$$\leq \frac{8\pi^2}{\lambda^2} \sum_{k=1}^K L_k^t \left(\left(\|\hat{\mathbf{W}}\|_{mj} \right) + \sqrt{M} \delta_{mj} \|\hat{\mathbf{W}}\|_2 \right) \times \left\| \boldsymbol{\Sigma}_k^H \bar{\mathbf{F}}_k \bar{\boldsymbol{\Phi}}_k (\mathbf{I} + \bar{\boldsymbol{\Gamma}}_k) \bar{\boldsymbol{\Phi}}_k^H \bar{\mathbf{F}}_k^H \boldsymbol{\Sigma}_k \right\|_2 + \delta_{mj} \sqrt{\frac{\alpha_k}{L_k^t}} \left\| [\bar{\mathbf{W}}_k]_m (\mathbf{I} + \bar{\boldsymbol{\Gamma}}_k) \bar{\boldsymbol{\Phi}}_k^H \bar{\mathbf{F}}_k^H \boldsymbol{\Sigma}_k^H \right\|_2 \triangleq \gamma_{mj}^{\text{Tx}}. \quad (84b)$$

$$\left\| [\mathbf{D}_k^{\text{Tx}}]_m \right\|_2 \leq \sqrt{\alpha_k} \left\| [\bar{\mathbf{W}}_k]_m (\mathbf{I} + \bar{\boldsymbol{\Gamma}}_k) \bar{\boldsymbol{\Phi}}_k^H \bar{\mathbf{F}}_k^H \boldsymbol{\Sigma}_k^H \right\|_2 + \sqrt{ML_k^t} \left\| \hat{\mathbf{W}} \right\|_2 \left\| \boldsymbol{\Sigma}_k^H \bar{\mathbf{F}}_k \bar{\boldsymbol{\Phi}}_k (\mathbf{I} + \bar{\boldsymbol{\Gamma}}_k) \bar{\boldsymbol{\Phi}}_k^H \bar{\mathbf{F}}_k^H \boldsymbol{\Sigma}_k \right\|_F. \quad (85)$$

of $\lambda_{\max} \left(\nabla_{\text{vec}(\mathbf{T})}^2 f_{\text{Quad}}(\mathbf{T}) \right)$ is obtained by computing the upper bound of $\left\| \nabla_{\text{vec}(\mathbf{T})}^2 f_{\text{Quad}}(\mathbf{T}) \right\|_{\infty}$, given by

$$\lambda_{\max} \left(\nabla_{\text{vec}(\mathbf{T})}^2 f_{\text{Quad}}(\mathbf{T}) \right) \leq \left\| \nabla_{\text{vec}(\mathbf{T})}^2 f_{\text{Quad}}(\mathbf{T}) \right\|_{\infty} \leq \max_{1 \leq m \leq M} 3 \sum_{j=1}^M \gamma_{mj}^{\text{Tx}} = \delta^{\text{Tx}}, \quad (86)$$

where we set δ^{Tx} as the r.h.s. of the second inequality in (86) since it is both tractable and greater than the l.h.s. of (26). Thus, the equation (31) is obtained by plugging (84b) into (86).

REFERENCES

- [1] K. B. Letaief, Y. Shi, J. Lu, and J. Lu, "Edge artificial intelligence for 6G: Vision, enabling technologies, and applications," *IEEE J. Sel. Areas Commun.*, vol. 40, no. 1, pp. 5–36, Jan. 2022.
- [2] W. Saad, M. Bennis, and M. Chen, "A vision of 6G wireless systems: Applications, trends, technologies, and open research problems," *IEEE Netw.*, vol. 34, no. 3, pp. 134–142, May 2020.
- [3] K. B. Letaief, W. Chen, Y. Shi, J. Zhang, and Y.-J. A. Zhang, "The roadmap to 6G: AI empowered wireless networks," *IEEE Commun. Mag.*, vol. 57, no. 8, pp. 84–90, Aug. 2019.
- [4] C.-X. Wang, X. You, X. Gao *et al.*, "On the road to 6G: Visions, requirements, key technologies, and testbeds," *IEEE Commun. Surveys Tuts.*, vol. 25, no. 2, pp. 905–974, 2nd Quarter 2023.
- [5] L. Lu, G. Y. Li, A. L. Swindlehurst, A. Ashikhmin, and R. Zhang, "An overview of massive MIMO: Benefits and challenges," *IEEE J. Sel. Topics Signal Process.*, vol. 8, no. 5, pp. 742–758, Oct. 2014.
- [6] G. J. Foschini and M. J. Gans, "On limits of wireless communications in a fading environment when using multiple antennas," *Wirel. Pers. Commun.*, vol. 6, pp. 311–335, Mar. 1998.
- [7] L. Zheng and D. Tse, "Diversity and multiplexing: A fundamental tradeoff in multiple-antenna channels," *IEEE Trans. Inf. Theory*, vol. 49, no. 5, pp. 1073–1096, May 2003.
- [8] K.-K. Wong, K.-F. Tong, Y. Zhang, and Z. Zhongbin, "Fluid antenna system for 6G: When Bruce Lee inspires wireless communications," *IET Electron. Lett.*, vol. 56, no. 24, pp. 1288–1290, Nov. 2020.
- [9] K.-K. Wong, A. Shojaeifard, K.-F. Tong, and Y. Zhang, "Fluid antenna systems," *IEEE Trans. Wireless Commun.*, vol. 20, no. 3, pp. 1950–1962, Mar. 2021.
- [10] W. K. New, K.-K. Wong, H. Xu, K.-F. Tong, and C.-B. Chae, "An information-theoretic characterization of MIMO-FAS: Optimization, diversity-multiplexing tradeoff and q-outage capacity," *IEEE Trans. Wireless Commun.*, vol. 23, no. 6, pp. 5541–5556, Jun. 2024.
- [11] K.-K. Wong, K.-F. Tong, Y. Chen, Y. Zhang, and C.-B. Chae, "Opportunistic fluid antenna multiple access," *IEEE Trans. Wireless Commun.*, vol. 22, no. 11, pp. 7819–7833, Nov. 2023.
- [12] L. Zhu, W. Ma, B. Ning, and R. Zhang, "Movable-antenna enhanced multiuser communication via antenna position optimization," *IEEE Trans. Wireless Commun.*, vol. 23, no. 7, pp. 7214–7229, Jul. 2024.
- [13] W. K. New, K.-K. Wong, H. Xu *et al.*, "A tutorial on fluid antenna system for 6G networks: Encompassing communication theory, optimization methods and hardware designs," *IEEE Commun. Surveys Tuts.*, 2024, early access, doi: [10.1109/COMST.2024.3498855](https://doi.org/10.1109/COMST.2024.3498855).
- [14] S. Song and R. D. Murch, "An efficient approach for optimizing frequency reconfigurable pixel antennas using genetic algorithms," *IEEE Trans. Antennas Propag.*, vol. 62, no. 2, pp. 609–620, Feb. 2014.
- [15] W. K. New, K.-K. Wong, H. Xu, K.-F. Tong, and C.-B. Chae, "Fluid antenna system: New insights on outage probability and diversity gain," *IEEE Wireless Commun. Lett.*, vol. 23, no. 1, pp. 128–140, Jan. 2024.
- [16] C. Psomas, G. M. Kraidy, K.-K. Wong, and I. Krikidis, "On the diversity and coded modulation design of fluid antenna systems," *IEEE Wireless Commun. Lett.*, vol. 23, no. 3, pp. 2082–2096, Mar. 2024.
- [17] K.-K. Wong and K.-F. Tong, "Fluid antenna multiple access," *IEEE Wireless Commun. Lett.*, vol. 21, no. 7, pp. 4801–4815, Jul. 2022.
- [18] K.-K. Wong, D. Morales-Jimenez, K.-F. Tong, and C.-B. Chae, "Slow fluid antenna multiple access," *IEEE Wireless Commun. Lett.*, vol. 71, no. 5, pp. 2831–2846, May 2023.
- [19] K.-K. Wong, K.-F. Tong, Y. Chen, Y. Zhang, and C.-B. Chae, "Opportunistic fluid antenna multiple access," *IEEE Wireless Commun. Lett.*, vol. 22, no. 11, pp. 7819–7833, Nov. 2023.
- [20] J. O. Martínez, J. R. Rodríguez, Y. Shen, K.-F. Tong, K.-K. Wong, and A. G. Armada, "Toward liquid reconfigurable antenna arrays for wireless communications," *IEEE Commun. Mag.*, vol. 60, no. 12, pp. 145–151, Dec. 2022.
- [21] H. Wang, Y. Shen, K.-F. Tong, and K.-K. Wong, "Continuous electrowetting surface-wave fluid antenna for mobile communications," in *Proc. IEEE Region 10 Conference (TENCON)*, Nov. 2022, pp. 1–4.
- [22] W. Ma, L. Zhu, and R. Zhang, "Capacity maximization for movable antenna enabled MIMO communication," in *Proc. IEEE Int. Conf. Commun. (ICC)*, Oct. 2023, pp. 5953–5958.
- [23] —, "MIMO capacity characterization for movable antenna systems," *IEEE Trans. Wireless Commun.*, vol. 23, no. 4, pp. 3392–3407, Apr. 2024.
- [24] L. Zhu, W. Ma, and R. Zhang, "Modeling and performance analysis for movable antenna enabled wireless communications," *IEEE Trans. Wireless Commun.*, vol. 23, no. 6, pp. 6234–6250, Jun. 2024.
- [25] J. Tang, C. Pan, Y. Zhang, H. Ren, and K. Wang, "Secure MIMO communication relying on movable antennas," *IEEE Trans. Commun.*, 2024, early access, doi: [10.1109/TCOMM.2024.3465369](https://doi.org/10.1109/TCOMM.2024.3465369).
- [26] B. Feng, Y. Wu, X.-G. Xia, and C. Xiao, "Weighted sum-rate maximization for movable antenna-enhanced wireless networks," *IEEE Commun. Lett.*, vol. 13, no. 6, pp. 1770–1774, Jun. 2024.
- [27] K. Shen and W. Yu, "Fractional programming for communication systems—Part I: Power control and beamforming," *IEEE Trans. Signal Process.*, vol. 66, no. 10, pp. 2616–2630, Mar. 2018.
- [28] —, "Fractional programming for communication systems—Part II: Uplink scheduling via matching," *IEEE Trans. Signal Process.*, vol. 66, no. 10, pp. 2631–2644, Mar. 2018.
- [29] X. Zhao, M. Li, Y. Liu, T.-H. Chang, and Q. Shi, "Communication-efficient decentralized linear precoding for massive MU-MIMO systems," *IEEE Trans. Signal Process.*, vol. 71, pp. 4045–4059, Oct. 2023.
- [30] Z. Zhang, Z. Zhao, K. Shen, D. P. Palomar, and W. Yu, "Discerning and enhancing the weighted sum-rate maximization algorithms in communications," *arXiv preprint arXiv: 2311.04546*, Nov. 2023.
- [31] K. Shen, Z. Zhao, Y. Chen, Z. Zhang, and H. Victor Cheng, "Accelerating quadratic transform and WMMSE," *IEEE J. Sel. Areas Commun.*, vol. 42, no. 11, pp. 3110–3124, Nov. 2024.
- [32] S. Vishwanath, N. Jindal, and A. Goldsmith, "On the capacity of multiple input multiple output broadcast channels," in *Proc. IEEE Int. Conf. Commun. (ICC)*, Apr. 2002, pp. 1444–1450.
- [33] V. Stankovic and M. Haardt, "Generalized design of multi-user MIMO precoding matrices," *IEEE Trans. Wireless Commun.*, vol. 7, no. 3, pp. 953–961, Mar. 2008.
- [34] K. Shen, W. Yu, L. Zhao, and D. P. Palomar, "Optimization of MIMO device-to-device networks via matrix fractional programming: A minorization-maximization approach," *IEEE/ACM Trans. Netw.*, vol. 27, no. 5, pp. 2164–2177, Oct. 2019.
- [35] S. Boyd and L. Vandenberghe, *Convex optimization*. Cambridge, UK: Cambridge University Press, 2004.
- [36] Y. Sun, P. Babu, and D. P. Palomar, "Majorization-minimization algorithms in signal processing, communications, and machine learning," *IEEE Trans. Signal Process.*, vol. 65, no. 3, pp. 794–816, Feb. 2017.
- [37] Z. Dong, Z. Zhou, Z. Xiao *et al.*, "Movable antenna for wireless communications: Prototyping and experimental results," *arXiv preprint arXiv: 2408.08588*, Aug. 2024.
- [38] B. Ning, S. Yang, Y. Wu *et al.*, "Movable antenna-enhanced wireless communications: General architectures and implementation methods," *arXiv preprint arXiv: 2407.15448*, Aug. 2024.
- [39] Y. Nesterov, *Lectures on Convex Optimization*. Cham: Springer, 2018.
- [40] R. A. Horn and C. R. Johnson, *Matrix analysis*. New York, NY: Cambridge university press, 2012.